Identifying Cosmic Ray induced Cascade events with IceTop

Kiran Munawar

December 11, 2017

A thesis presented for the degree of Master in Science at the

University of Canterbury

University of Canterbury,
Department of Physics and Astronomy,
Private Bag 4800, Christchurch, New Zealand.

Dedication

To my Uncle Asaph Mall.

ABSTRACT

IceCube is the largest neutrino detector in the world. It consists of an array of photomultiplier tubes installed throughout a cubic kilometre of ice below the surface at the South Pole. These photomultiplier tubes detect the Cherenkov radiation from neutrino-nucleon interactions. IceTop is the surface component of IceCube neutrino observatory and is used to study Cosmic Ray Extensive Air Showers (EAS). The goal of IceCube is to investigate astophysical neutrinos. However the majority of events recorded by IceCube are background events caused by cosmic rays interacting in the Earth's atmosphere. This thesis is concerned with developing a technique to veto the background events from the IceCube experimental data using the IceTop surface array.

Four original studies were performed. In the first study the output of a cosmic-ray air shower simulation code was compared with real events detected by IceCube and IceTop. It was found that the simulation code performed well, although in some cases the actual number of hits detected in IceTop ws greater than predicted. However as far as assessing the ability of IceTop as a veto this means our estimates will be conservative which would mean that the veto would be more effective than estimated. In the second study the cosmic-ray simulation code was used to investigate the scope of background events which might be able to vetoed using the IceTop array and the energies and zenith angles where the veto would be effective were given. The appropriate time window for deciding whether an IceTop hit was related to an event detected in the IceCube detector was investigated in the third study and was found to be -500 ns to 800 ns relative to the timing of the IceCube event. In the fourth study, the final sample of a published IceCube cascade analysis was examined to determine whether there were any related hits in the IceTop array.

Contents

List of Figures

Acronyms

ATWD Analog Transient Waveform Digitizer

AGNs Actice Galactic Nuclei

CC Charged Current

CORSIKA Cosmic Ray SImulations for KAscade

CMB Cosmic Microwave Background

DOM Digital Optical Module

EAS Extensive air showers

EHE Extremely High Energy

EM Electromagnetic

eV Electron Volt

fADC fast Analog-to-Digital Converter

GRBs Gamma Ray Bursts

HG High gain

IBD Inverse Beta Decay

IC IceCube

IT IceTop

LDFs Lateral Distribution Functions

LG Low gain

NC Neutral Current

PMT Photomultiplier Tube

SNRs SuperNova Remnants

VEM Vertical equivalend muons

UHECR Ultra High Energy Cosmic Rays

1 Introduction

Neutrinos are fundamental particles with no electric charge. Because they are electrically neutral, neutrinos are not affected by electromagnetic forces. This makes them challenging to detect, but also means they are ideal astronomical messenger particles as they can travel across the Universe without interference or being absorbed by matter. Unlike charged particles, whose trajectories are affected by magnetic fields, neutrinos can point back to their source and identify the sites in the Universe, where particles are accelerated to high energies. Observation of these neutrinos provides valuable information about the particle production mechanism in the astrophysical sources. However, the fact that neutrinos have a very small probability to interact, means that a large volume detector is required to detect them.

IceCube is the world's largest neutrino detector. It has been constructed at the South Pole in Antarctica and consists of a total of over 5000 optical sensors installed between 1450 and 2450 meters below the surface of the ice. These sensors detect the optical Cherenkov light emitted by the charged particles produced when neutrinos interact in the ice.

The primary goal of IceCube is to search for very high energy astrophysical neutrinos. However the majority of events recorded are not the events sought, but background events from cosmic rays interacting in the Earth's atmosphere. When cosmic rays interact with molecules in the Earth's atmosphere, they produce the majority of the background to all astrophysical neutrino searches in the form of atmospheric muons and atmospheric neutrinos. The background events are about a factor of 10^6 more numerous than astrophysical neutrino events and their removal necessitates the use of filtering and veto techniques. Most of the techniques

currently in use rely solely on the information from the optical sensors in the ice and exploit the differences in direction, and the light distribution, between signal and background events.

In addition to the optical sensors deep in the ice, the IceCube observatory includes an array of detectors on the surface called IceTop. IceTop is designed to detect the charged particles produced when a cosmic ray interacts in the atmosphere, in order to study the energy spectrum and composition of cosmic rays.

In this thesis the use of IceTop as a veto to identify background events in IceCube is investigated. As explained above, the background events are muons, produced by cosmic ray interactions in the atmosphere. Muons with sufficient energy are able to penetrate the ice and produce Cherenkov light in the deep neutrino detector. Such background events are accompanied by air showers of particles which, depending on the shower orientation and surface intercept, may be detected by the IceTop sensors. IceCube events which have correlated events in IceTop can be removed from the data set, as signal events should not have any IceTop correlations. This technique is an example of a veto technique.

The use of IceTop as a veto is limited by the size of IceTop and the fact that IceTop does not extend beyond the cross-sectional area of the IceCube neutrino sensors. Recently reported evidence of an astrophysical neutrino flux [7] has motivated the possibility of construction of an extended surface array. This is particularly to extend the sensitivity of IceCube to neutrinos from the Southern Hemisphere, where the background from atmospheric muons is most limiting [1]. One possibility to get rid of this background is an extended surface detector, which could allow the rejection of a large fraction of atmospheric backgrounds muons as well as neutrinos from the same air shower. The IceCube collaboration is currently investigating a new generation IceCube detector, referred to as IceCube-Gen2 [8], which would build upon the current IceCube neutrino detector infrastructure to improve the results that are obtained. Some IceCube Gen-2 plans include a larger surface array extended to large areas of several km^2. The large area of the surface array will be more efficient than IceTop in detecting the cosmic-ray air showers and vetoing the muons and neutrinos produced in the atmosphere. The techniques developed, and investigated in this thesis, will help inform the Gen-2 project.

[1] Atmospheric muons cannot penetrate the entire diameter of the Earth and so true upward going events must have a neutrino origin; such neutrinos can be either atmospheric or astrophysical neutrinos.

1.1 Introduction to Neutrinos

Neutrinos are the only fundamental fermions which have no electric charge. As neutrinos do not have electric charge they do not have electromagnetic interactions and participate only in weak processes with virtual $W^{\pm}$ and Z^0 bosons (like β-decay of nuclei, inverse β process $\bar{\nu}_e$ + p $\rightarrow e^+$n, etc.). There are three types of neutrinos. Each type of neutrino is associated to a charged particle. For example, "electron neutrino" is linked with electron, and muon and tau neutrinos are related to the muon and tau respectively.

The neutrino was first postulated by Wolfgang Pauli in 1930 in a famous letter addressed to participants of a nuclear conference in T*ü*bingen. Pauli proposed the existence of a new particle in order to make sense of the radioactive-disintegration mode known as beta decay [9]. In radioactive decay processes the only detected product particles were the daughter nucleus and an electron. However the emitted electron was noticed to have a wide ranging energy spectrum. This shouldn't have been the case if there were only two daughter particles produced in the decay, but could be possible if there were three decay products. In order to save the energy and charge conservation principles, Pauli proposed that this unseen particle should be neutral and had to have a very small mass. Pauli received the Nobel Prize in 1945.

The experimental verification of the existence of neutrino was made in 1956 by Fred Reines and Clyde Cowan. In 1951 Reines and Cowan [10] detected a free neutrino by observing its inverse beta-decay interaction (IBD). In an IBD process a free neutrino interacts with the matter and is stopped; a neutrino interaction with a neutron would produce a proton and an electron. A neutrino interaction with a proton would yield a neutron and a positron, a positively-charged electron. The detection of the neutrino was as the initiator of the inverse-beta decay reaction of:

$$\bar{\nu} + p \rightarrow n + e^+. \tag{1.1}$$

Since then neutrinos with a large range of energy and from many sources have been detected. These include neutrinos from the centre of the Sun; from radioactive processes deep within the crust of the Earth; from cosmic-ray interactions in the Earth's atmosphere and from particles accelerated in man-made accelerators.

The IceCube neutrino detector was designed to detect the TeV, and greater, energy astrophysical neutrinos produced in association with cosmic rays. Such astrophys-

ical neutrinos are expected to be produced when cosmic rays interact with matter or radiation close to their production site. Neutrinos point back to their origins while the trajectories of the charged cosmic rays are bent in magnetic fields and so a key goal for IceCube is to determine the origin of the highest energy cosmic rays through detecting the astrophysical neutrinos associated with them. The first evidence for a flux of astrophysical neutrinos inconsistent with the expectation from atmospheric backgrounds at greater than 5σ was published by IceCube in 2014 [7]. No significant anisotropy has been observed in the flux and currently there are no known astrophysical objects which have been related to the observed neutrinos. With greater neutrino event numbers the chance of determining the neutrino sources increases. This project aims to improve the efficiency of retaining signal neutrino events through the use of the IceTop array in the background filtering process. IceCube neutrino events can be classified by their light pattern as will be discussed in section 3.3. This thesis is dedicated to investigate the probability to veto cosmic ray air shower, using the IceTop air shower array, to isolate astrophysical neutrino events of the cascade classification.

This thesis describes four separate original studies. The first study compared the output of a cosmic-ray air shower simulation code with data. In the second study the cosmic-ray simulation code was used to investigate the scope of background events which might be able to vetoed using the IceTop array. In the third study the appropriate time window for deciding whether an IceTop hit was related to an event detected in the IceCube detector was investigated. In the fourth study, the final sample of a published IceCube cascade analysis was examined to determine whether there were any related hits in the IceTop array.

The thesis is presented as follows. Chapter 2 introduces cosmic rays along with their sources and acceleration mechanisms and the Heitler model, which gives a relatively simple approach to predict the properties of extensive air showers. Chapter 3 describes IceCube, the IceTop air shower detector array, the IceCube method of detecting neutrinos, and its analysis strategies. Chapter 4 presents the simulation code which is used in this thesis for simulating cosmic ray extensive air showers and my study comparing the output of this code with experimental data. Chapter 5 discusses the potential for the use of IceTop veto and describes my study investigating the scope using the air shower simulation code and my study into an appropriate time window to define correlations between IceTop and IceCube. Chapter 6 is devoted to my fourth study examining whether there were any related IceTop array hits in the final events of a published IceCube analysis. Chapter 7 provides a summary of the results from this research project and discusses future directions for this research.

2

Cosmic Rays and Extensive Air Showers

In this chapter, cosmic rays are introduced. Firstly, cosmic ray acceleration mechanisms and their expected sources are discussed. This is relevant for the IceCube observatory as its main goal is to illuminate the origin of cosmic rays through studying the associated astrophysical neutrinos. Secondly, the properties of the cosmic rays and the air showers which are generated in the atmosphere are discussed. These properties are needed in order to be able to understand how to reduce the cosmic ray background for neutrino detection.

Cosmic rays are high-energy charged particles; about 90% protons, 9% alpha particles and the rest are heavier nuclei [11]. They are highly relativistic and bombard the Earth at the rate of about 1000 per square metre. They were discovered in 1912 by an Austrian physicist Victor Hess in his balloon experiment (see figure 2.1). For this discovery Hess received the 1936 Nobel prize in physics.

Ultra High Energy Cosmic Rays (UHECR) are the most energetic particles observed in Nature, with energies over 10^{20} eV. There is no known mechanism, in the universe, capable of accelerating these particles to such high energies. Regardless of the distribution of their sources in the sky cosmic rays arrive from all directions, because they are charged and therefore their directions are randomized by the deflection from magnetic fields. The sources of these high energy charged particles has been a mystery for many years.

Recent analysis of gamma-rays detected by the Fermi-Lat detector has provided evidence that supernova remnants in our own galaxy accelerate cosmic rays in the GeV (10^9 eV) energy range [12]. A supernova explosion is a transient source of energy. During a short time interval a supernova can radiate as much energy as

the Sun is expected to emit over its entire life span. Supernovae are responsible for the distribution of heavy elements throughout the Universe and their remnants have long been considered the major source of galactic cosmic rays. The supernova remnant is the ejected material which expands as a shock wave into the interstellar medium.

These supernova remnants are also targeted by neutrino telescopes. However the main focus for telescopes such as IceCube is to identify the source of the cosmic rays with energies greater than 10^{15} eV. These cosmic rays are not believed to be accelerated in supernova remnants for the spatial size of the accelerating regions is smaller than the gyroradius particles with energies greater than 10^{15} eV.

Figure 2.1: Hess in August 1912 after one of his successful balloon flights in which he observed an ionization increase with altitude.

2.1 Cosmic-ray Energy Spectrum

According to the measurements from different experiments, see figure 2.2, the cosmic ray energy spectrum follows a power-law relation of $dN/dE \propto E^{-\gamma}$. The spectrum steepens from $E^{-2.7}$ to $\sim E^{-3}$ at energy about 10^{15} eV. This feature is known as "knee" of the spectrum and was first discussed by Kulikov and Khristiansen in 1958 [13]. Furthermore, the spectrum shows another feature at energies 3×10^{18} eV and named as "ankle" of the spectrum [14]. The steepening of the cosmic ray spectrum at the knee is considered to be an indicator of the upper end of galactic sources of cosmic rays. It corresponds to the maximum energy that a proton can have in most galactic acceleration mechanisms. Above the ankle the spectrum hardens again and the cosmic rays in this region are believed to be coming from extragalactic origin. As the gyroradius of a particle at energies above 10^{19}

eV is of the order of the dimension of the galaxy and such high energy cosmic rays cannot belong to our galaxy. They have to be coming from a huge and powerful extra-galactic sources. At energies above 6×10^{19} eV, a strong suppression in the cosmic ray energy is observed. This cutoff is referred to as the GZK cutoff (see below for more details and acronym meaning). At energies higher than the GZK cutoff, cosmic ray particles lose energy through their interaction with the cosmic microwave background.

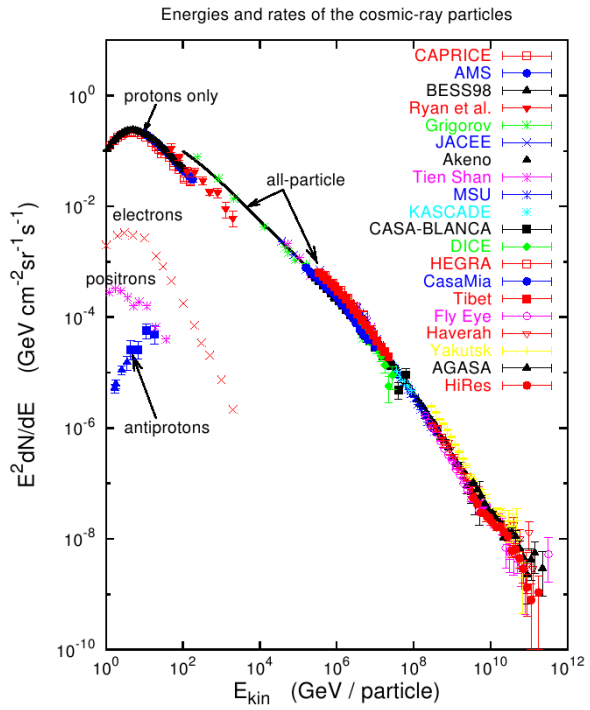

Figure 2.2: The spectrum of cosmic rays measured by various experiments. There are two prominent features in the spectrum: the "knee" at 10^{15} eV and the "ankle" at about 10^{18} eV. The figure is taken from [1].

2.2 Propagation through space

Cosmic rays can have travelled cosmological distances before they are detected by cosmic ray detectors. During their propagation from the source to the detector, they interact with magnetic fields, background photon and the dust particles. Therefore, the energy spectrum and element composition of the cosmic rays on the Earth are not the same as at the source. Many propagation models have been

developed to explain cosmic ray propagation in the Universe. More details about the cosmic ray acceleration is given in [11, 15].

A study of the ratio of secondary to primary cosmic-ray nuclei reveals that propagation effects of charged particles through the galaxy adds an energy dependence of $E^{-0.6}$ to the source spectrum of charged cosmic rays [14]. A source energy spectrum of E^{-2}, as will be explained in section 2.3, together with a propagation spectrum is in good agreement with the observation of the cosmic-ray spectral index of -2.7.

2.2.1 GZK Cutoff

At energies $E > 10^{19}$ eV, a suppression in the cosmic rays flux was predicted in 1966 by Greisen [16] and Zatsepin and Kuzmin [17] and called the GZK cutoff. This prediction assumes that the extragalactic component of the spectrum contains only protons which interact with the cosmic microwave background photons (CMB) via photo-pion production. This energy-loss mechanism limits the range of cosmic protons above the threshold to less than ~ 50 Mpc.

The dominant interactions of protons with the CMB are:

$$p + \gamma_{CMB} \rightarrow \Delta^{+} \rightarrow n + \pi^{+} \tag{2.1}$$

$$p + \gamma_{CMB} \rightarrow \Delta^{+} \rightarrow n + \pi^{0}.$$

Measurements from [18] showed a cutoff in the flux at the predicted cutoff energy.

2.3 Acceleration Mechanism

The origin of cosmic rays and the mechanism which accelerates particles to such high energies have been subject to debate for many years [19]. It is generally believed that low energy cosmic rays are from galactic sources and those with the highest energies are extra-galactic in origin.

2.3.1 Fermi Acceleration

In 1949 Enrico Fermi [20] proposed the so-called Fermi acceleration mechanism in which a cosmic ray particle can be accelerated and gain energy by collision with moving magnetic clouds or shockwaves in the interstellar space over a long period of time. In this acceleration mechanism a charged particle experience a multiple electromagnetic scattering in ionized gas clouds which are present in the surrounding of astrophysical objects. The iterative scattering of charged particles becomes more effective in the presence of astrophysical shocks. Figure 2.3 illustrates a shock moving with velocity $-\vec{u}_1$ in the laboratory frame.

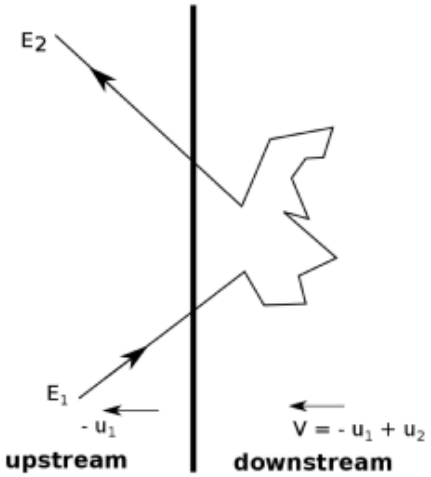

Figure 2.3: Acceleration at a shock front. The figure is taken from [11].

Particles move back and forth in the upstream and downstream region. After each crossing of the shock front by a charged particle gains an average relative energy of $\Delta E/E = \xi$. After n encounters, the energy of the particle will be [11]:

$$E_n = E_0(1+\xi)^n. \tag{2.2}$$

where E_0 is the energy at injection point into the acceleration, ξ is the relative energy gain and n is defined as:

$$n = \ln\left(\frac{E}{E_0}\right) / \ln(1+\xi). \tag{2.3}$$

After each encounter the probability of a particle to leave the acceleration region is P_{esc}. After the particle has escaped it cannot be accelerated further. Therefore, the number of particles reaching energies larger than a given energy E is given by:

$$N(\geq E) \propto \sum_{m=n}^{\infty}(1-P_{esc})^m = \frac{(1-P_{esc})^n}{P_{esc}} \tag{2.4}$$

$$N(> E) \propto \frac{1}{P_{esc}}\left(\frac{E}{E_0}\right)^{-\gamma}. \tag{2.5}$$

with spectral index

$$\gamma = \ln\left(\frac{1}{1-P_{esc}}\right) / \ln(1+\xi) \approx \frac{P_{esc}}{\xi}. \tag{2.6}$$

The energy spectrum of the cosmic rays depends on the conditions of the acceleration effects and generically leads to a spectral index of -2.0.

However, individual source spectra can vary depending on the conditions of the cosmic ray sources. Simulation of astrophysical shocks show that spectral index strongly rely on the shock boost factor Γ, shock multiplicity and orientation between particles and shock fronts [21].

2.4 Source candidates

Many sites have been proposed for the acceleration of high-energy cosmic rays. In order to accelerate particles to high energies, powerful shocks and strong magnetic fields that can confine the particles within the accelerator's site, while being accelerated, are necessary. The probability of a particle to escape the region where it was being accelerated increases, if the particle's gyroradius is comparable to the size of the acceleration region. Once it is no longer trapped in the acceleration region the particle will be unable to gain more energy. This maximum achievable energy by the accelerated particle can be expressed by Hillas criterion [22]. Hillas criterion, obtained from the expression for the gyroradius of a particle electric charge q in a magnetic field B, is

$$\varepsilon_{max} = qBR, \tag{2.7}$$

where R is the size of the accelerator.

This relation is graphically illustrated by Hillas plot in figure 2.4. In this plot several types of astrophysical objects are shown according to their ability to accelerate cosmic rays up to energies of 10^{20} eV or higher. Sources must be above the upper diagonal line to accelerate protons to more than 10^{20} eV. The blue dotted lines indicate the lower limits of the bands if iron nuclei are to be accelerated to 10^{20} eV instead of protons.

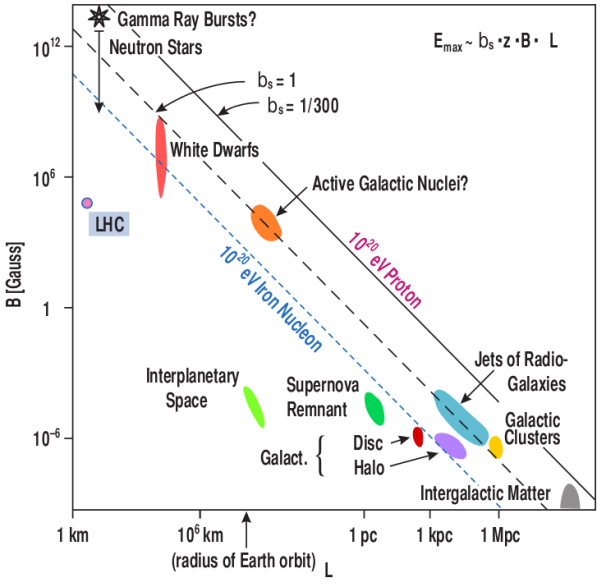

Figure 2.4: Estimated size and magnetic field strength of sites where cosmic rays might possibly be accelerated to ultra-high energies. Adopted from [2].

2.4.1 Galactic source candidates

Supernova remnants (SNRs), shown in Figure 2.5, are considered the primary origin of the galactic cosmic rays below 10^{18} eV [23]. Supernova explosion happens when a burned out star gravitationally collapse into a neutron star or black hole. As a result of the explosion, supernova remnants spread out into the interstellar medium. This is an excellent environment for the shock acceleration of the cosmic rays.

As mentioned in the preamble to this chapter,the Fermi collaboration has recently reported the gamma ray emission, which is consistent with the neutral pion decays,

from the galactic SNRs [12]. This shows the evidence of hadronic acceleration in SNRs. The objects which can emit VHE gamma rays, can also be the sources of cosmic ray acceleration.

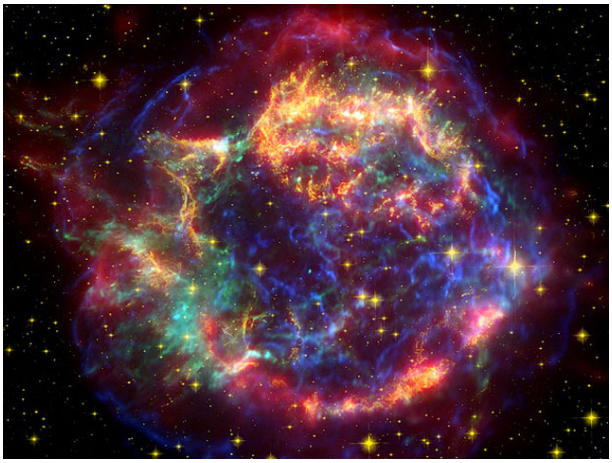

Figure 2.5: This image of Cassiopeia A, a 325 years old supernova remnant, is taken from NASA's observatories [3].

2.4.2 Extragalactic source candidates

The sources for the highest energy cosmic rays are expected to be extragalactic in nature and the most popular candidates proposed are active galactic nuclei (AGNs) and gamma-ray bursts (GRBs).

Active Galactic Nuclei, shown in Figure 2.6, the most powerful objects in the physical universe, are suggested to be a possible source of extragalactic cosmic rays. The galaxies contain a supermassive rotating black hole in their centre. The black hole is accreting matter from the accretion disk. The accretion disk is fed by matter from a dust torus. Perpendicular to the accretion disk, two relativistic jets are responsible for emitting radiation and transporting matter from the core to the outside. Knots and hot spots along the jets emit strong radio emission, observed from AGNs. These knots and hot spots are ideal for shock environments in which charge particles are accelerated to high energies [4].

Gamma Ray Bursts are among the most luminous phenomena known in the universe. They were first discovered by the Vela satellite in 1967 [24]. Gamma Ray Bursts emit energies of the order of 10^{51} erg in few seconds, which are comparable to the Sun's emission during its entire lifetime. The explosion of a GRB leads to

the formation of multiple shock regions which are potential acceleration sources for ultra high cosmic rays (UHECRs). The fireball model describes a generic scenario [25] for the formation of shock environments for stochastic acceleration and predicts energy spectra for the accelerated particles.

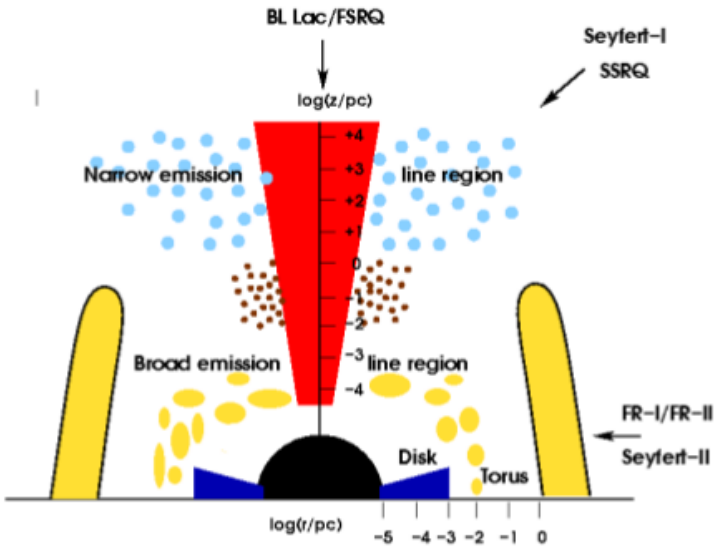

Figure 2.6: Schematic view of AGN. The black hole at the centre is surrounded by the accretion disk and the jets are perpendicular to the disk. The torus surrounds the whole layout. Figure is taken from [4].

2.5 Cosmic ray induced background events for neutrino searches

Cosmic rays, after entering the Earth's atmosphere, interact with the air molecules and initiate a cascade of particle showers. These particle showers mostly contain photons, muons, electrons, pions, and neutrinos. The highest energy atmospheric muons can penetrate the ice to the depth of IceCube and along with the neutrinos act as a background to all astrophysical neutrino searches. To be able to remove and model this background, the study of cosmic ray interactions in the atmosphere is important.

2.6 Extensive Air Showers

Cosmic ray air showers, called extensive air showers (EAS), are the cascade of particles which are produced when a cosmic ray particle interacts with an air molecule in our atmosphere, see Fig 2.7. If the energy of the primary cosmic ray particle is high enough, the secondary particles produced in the shower will penetrate the atmosphere to the ground level where they can be detected using ground base detectors to infer the properties of primary cosmic ray particle [26]. As an indication of the shower numbers and particle content of the shower, a cosmic ray proton of energy 1 PeV can produce about 10^6 secondary particles at sea level, with around 80% photons, 18% electrons, 1.7% muons and about 0.3% hadrons.

Extensive air shower development in the atmosphere depends on the nature of the interactions (hadronic and electromagnetic) and decay properties of the particles. Extensive air showers develop as a combination of three components: hadronic, muonic and electromagnetic [11]. Normally, the electromagnetic particles produced in the extensive air shower are referred to as "soft component" of the air shower because they get stopped by the surface due to their energy loss through ionization. Muons on the other hand have ability to penetrate through the surface for a notable distance and are therefore referred to as the "hard component" of the air shower.

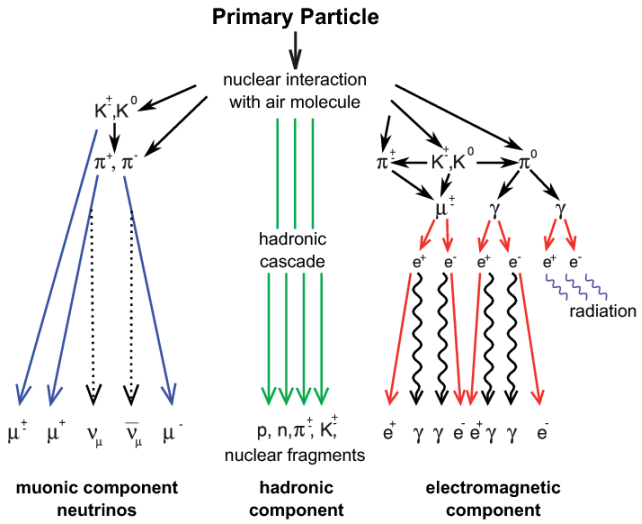

Figure 2.7: Symbolic representation of EAS. Here blue represents the muonic, green hadronic and red the electromagnetic components of the shower.

In 1937 Walter Heitler along with Homi Bhabba provided an explanation for how the extensive air showers are initiated [27]. Heitler also explained how these showers are sustained [28]. In subsequent years, the theory had been updated by other researchers to match the current knowledge. The work by Matthews [5] and Horandel [29] is very important and their updated version is used for this project.

2.6.1 Electromagnetic component

The electromagnetic (EM) component of an air shower is initiated by photons and electrons, when they undergo bremsstrahlung and the pair production mechanism. The Heitler model [28] is a simple model which explains the basic features of the electromagnetic component of the air showers. According to the Heitler model, a particle (electron or photon) with energy E_{em} splits into two new particles, after a spitting length $d = X_0 \ln 2$, where X_0 is the radiation length of the medium, see Fig 2.8. The primary energy is supposed to be equally divided between the two produced particles; each secondary particle having energy $E = E_{em}/2$. After the second splitting length the number of secondary particles is 2^2, each with energy $E = E_{em}/2^2$. After n splitting lengths which will be after the distance $x = nX_0 \ln 2$, the shower contains $N = 2^n = e^{x/X_0}$ particles, each with energy $E = E_0/N$.

The cascade of these secondary particles continues to grow until the energy of the particles fall below the threshold energy E_c^{em}, which is usually called the characteristic energy, at which pair production or bremsstrahlung no longer occurs. At this stage, the average collisional energy losses begin to exceed radiative losses and the shower reaches its maximum size (maximum number of particles) X_{max}^{em} [26].

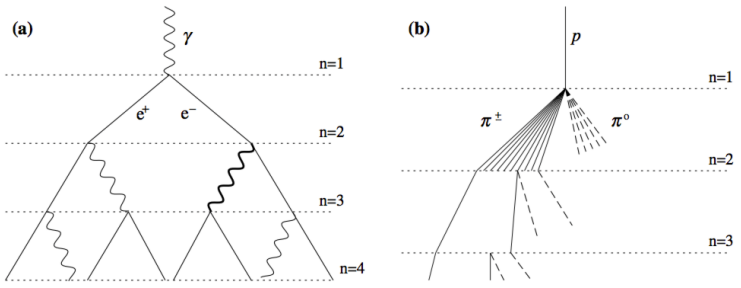

Figure 2.8: Heitler model for electromagnetic shower (a) and hadronic shower (b). Figure is taken from [5].

Following this process the shower will have maximum size when all of the daughter particles have the characteristic energy. The number of particles at the maximum shower development is then

$$N^e_{max} = \frac{E_{em}}{E^{em}_c} \tag{2.8}$$

where E^{em}_c, the characteristic energy of the electromagnetic component of the shower, normally takes the value of 87 MeV. The penetration distance where the shower reaches its maximum depth can be found by considering the number of splittings for the energy to be reduced to the characteristic energy. The number of splittings n_{spl} is related to N^e_{max} through $N^e_{max} = 2^n_{spl}$ meaning the penetration distance is

$$X^{em}_{max} = X_0 \ln\left(\frac{E_{em}}{E^{em}_c}\right). \tag{2.9}$$

where X_0, the radiation length in air has a typical value of around 36.66 g/cm^2.

This model was too simple, as Heitler himself had already noticed, because when bremstrahlung occurs usually more than one photon is produced and sometimes electrons and positrons range out and don't produce any photons. For this reason to characterize the simplification a correction factor g was introduced in equation 2.8

$$N^e_{max} = \frac{E_{em}}{gE^{em}_c}. \tag{2.10}$$

2.6.2 Hadronic showers

The showers which are initiated by mesons are referred to as "hadronic showers". The hadronic component of an air shower is the first generation of the secondary particles of the extensive air shower. The whole air shower development occurs around its dense hadronic core which is directed along the primary cosmic ray direction. The hadronic interactions include nucleon-nucleon, nucleon-nucleus and nucleus-nucleus inelastic collisions and also pion-nucleon and pion-nucleus interactions.

In a proton initiated extensive air shower the proton will interact with an air molecule and produce charged and neutral pions. Roughly 80% of the hadronic cascade produce pions. The neutral pions decay immediately into gamma rays through the following modes [14]:

$$\pi^0 \rightarrow \gamma + \gamma \qquad (98.8\%) \tag{2.11}$$

$$\pi^0 \rightarrow e^+ + e^- + \gamma \qquad (1.2\%)$$

The high energy gamma rays, produced as a result of the decay of these neutral pions, induce electromagnetic sub-showers by annihilating into electrons and positrons.

On the other hand, the charged pions will travel a layer of atmosphere and interact again with an air molecule. This in turn will produce more charged and neutral pions. This cascade of charged pions continues until the energy falls below a threshold energy E_c^π, at which point they decay to muons and thereby feed the muonic component through the following decay reaction:

$$\pi^\pm \rightarrow \mu^\pm + \nu_\mu/\overline{\nu_\mu}, \tag{2.12}$$

Following similar arguments as sued to derive the Heitler model similar relations as derived for electromagnetic showers, can be derived for hadronic showers. This model is called extended the Heitler model [5]. According to this model, the number of muons (N_{max}^μ), and electrons (N_{max}^e) at the maximum level of development (X_{max}^p) can be related to the primary energy according to:

$$N_{max}^\mu = \left(\frac{E_0}{E_c^\pi}\right)^\beta, \tag{2.13}$$

$$N_{max}^e = \left(\frac{a(E_c^\pi)^{-b}}{gE_c^{em}}\right) E_0^{1+b}, \tag{2.14}$$

$$X_{max}^p = X_{const} + \Lambda \ln\left(\frac{E_0}{PeV}\right). \tag{2.15}$$

Here, E_0 is the energy of the primary particle and E_c^π is the characteristic energy of pions. The constants a, b, β, X_{const} , and Λ relate to energy independent characteristics of the showers. The two constants, X_{const} and Λ , take the values of 412.1 g/cm^2 and 30.4 g/cm^2 respectively [30].

These relation are also oversimplified because of approximations and parametrisations that are used to reach conclusions. In reality, there are other factors that

must be taken into account to build stronger relations that more accurately describe extensive air showers. These more precise relations are described in the following section and are used for this project.

2.7 Empirical Relations

Although, the relations presented in the above section do provide an understanding of the mechanisms of extensive air showers, there are some factors that have been neglected and approximated. In order to consider these factors, the coefficients and powers involved in these relations must be fine-tuned. In this project we are interested in evaluating the particle content expected from various air showers to determine whether the air shower could be detected by the IceTop array. A simulation code which is described in Chapter 4 is used to evaluate the likelihood of IceTop receiving hits. In the subsections below, the expressions which are used in this simulation code are presented. The first of the subsections below describes how the mass distribution through the atmosphere is characterised in terms of the overburden. In the subsequent subsections, relations are given for the shower maximum position and number of particles and relations characterising the development of the shower in both the longitudinal and lateral dimensions.

2.7.1 Overburden

The mass distribution within the atmosphere, especially for downward oriented trajectories, can be describe in terms of the overburden. The overburden at an altitude z is defined as the integral of the density profile of $\rho(h)$ of the atmosphere for altitude h from sea-level:

$$X_v = \int_z^\infty \rho(h) dh. \tag{2.16}$$

In this project we are interested in evaluating the shower particle content at IceTop. The IceTop air shower array is located 2835m above sea level and this height must be included in order to calculate the overburden. The equation 2.16 can be parameterized specifically at the South Pole [31] by the following relation:

$$X_v = \begin{cases} 146.66 + 932.8 * \exp(-h/5208) & \text{if } 3960 \geq h > 0 \\ -110.33 + 1119.8 * \exp(-h/8255) & \text{if } 8530 \geq h > 3960 \\ -6.80 + 1182.0 * \exp(-h/6145) & \text{if } 17680 \geq h > 8530 \end{cases}$$

An inclined shower propagates through more atmosphere and therefore has a larger amount of overburden than a vertical shower. To account for the shower paths that are inclined to a surface by some zenith angle D_θ, the assumption of a flat Earth is taken. Thus, the overburden of a slanted path X_s is given by

$$X_s = \frac{X_v}{D_\theta}. \tag{2.17}$$

2.7.2 Position of shower maximum

As stated in the extended Heitler model, the position of the shower maximum for a hadronic shower can be described by equation 2.15.

According to the results obtained from IceTop, the constants X_{const} and Λ used in this equation take the values of 557.4 g/cm^2 and 25 g/cm^2 respectively in order to describe the position of the shower maximum more accurately [30].

2.7.3 Number of electrons and muons at maximum

According to extended Heitler model [5], in the hadron initiated shower the number of electrons and muons at the maximum follow power law relations of the primary energy E_0 as described by equations 2.14 and 2.13. In order to account for over-simplifications, assumptions, and comparisons to experimental data, one arrives at the expressions of the forms for electrons [32] and muons [30]:

$$N^e_{max} = 27.68 \times E_0^{1.13}, \tag{2.18}$$

$$N^\mu_{max} = 0.95 \times 10^5 \left(\frac{N^e_{max}}{10^6} \right)^{0.75}. \tag{2.19}$$

2.7.4 Longitudinal Development

Gaisser and Hillas developed a parametrisation that describes the electron distribution in the extensive air showers [33]. The derivation includes a number of shape parameters, in particular a first interaction term, an attenuation rate, and a term describing the maximum number of particles produced.

The general characteristics of air showers created by hadrons and photons relies on the physics of electromagnetic interaction. For this reason, after the publication of Gaisser and Hillas parametrisation, it was realised that this derivation can be applicable to muon development as well [34].

The parametrisations used in the simulation code used in this research are:

$$N_e(X_s) = N^e_{max}\left(\frac{X_s - X_0}{X_{max} - X_0}\right)^{\frac{X_{max}-X_0}{\lambda_e}} \exp\left(\frac{X_{max} - X_s}{\lambda_e}\right), \tag{2.20}$$

$$N_\mu(X_s) = N^\mu_{max}\left(\frac{X_s - (X_{max} + X^\mu_0)}{-X^\mu_0}\right)^{\frac{-X^\mu_0}{\lambda_\mu}} \exp\left(\frac{X_{max} - X_s}{\lambda_\mu}\right). \tag{2.21}$$

The above mentioned parametrisations contain seven constants(N^μ_{max}, N^e_{max}, X_{max}, X^μ_0, X_0, λ_μ, λ_e). Here X_0 describes the overburden of the first interaction of the particle, and is found to be around 100 g/cm^2. X^μ_0 is a shape parameter for the muon distribution and can be taken as -200 g/cm^2. The effective radiation lengths for electrons and muons are denoted by the constants λ_e and λ_μ respectively, with the values of $\lambda_e = 70$ g/cm^2 and $\lambda_\mu = 1109$ g/cm^2.

2.7.5 Lateral Development

Extensive air shower development on planes perpendicular to the shower core can be described by Lateral Distribution Functions (LDFs). One of the parametrisations for the Lateral Distribution Functions are known as Nishimura-Kamata-Greisen (NKG) functions. These curves are so named due to the publication of similar parametrisations by the three namesakes [35] [36]. The density of electrons and muons in units of particles per unit area can be derived from these functions and is defined as:

$$\rho_e = 0.4 \frac{N_e}{r_M^2} \left(\frac{r_M}{r} \right)^{0.75} \left(1 + \frac{r}{r_M} \right)^{-3.25} . \tag{2.22}$$

$$\rho_\mu = 1.89 * 10^{-4} N_\mu r^{-0.75} \left(1 + \frac{r}{320m} \right)^{-2.5} . \tag{2.23}$$

Here r_M represents the Moliere radius and at the South Pole takes the value of 105m. This value can be elucidated as the lateral distance from the shower core that encloses around 90% of the showers energy.

2.8 Cosmic ray air shower simulations

CORSIKA [37] is a Monte-Carlo simulation program which is used to study the properties and the development of extensive air showers produced by cosmic ray particles. CORSIKA tracks the secondary particles through the atmosphere and uses Monte-Carlo methods to simulate the possible interaction and decay outcomes according to the appropriate cross-sections and decay properties. All secondary particles are tracked and their arrival times, energies, locations and directions are stored when reaching a chosen detector. Each simulation run from CORSIKA provides a particular realisation of the possible particles arriving at the chosen detector. By running CORSIKA multiple times a distribution of many possible particle realisations can be built up, including extreme occurrences where for example an unusually high proportion of the initial energy is transferred to a secondary particle. A disadvantage in running CORSIKA is that the individual particle tracking means that the simulation is quite slow to run. CORSIKA is used by the IceCube collaboration to generate background events in the neutrino detector in the ice.

In contrast the simulation code used in this research project does not track individual particles but uses the parametrisations mentioned in the previous sections to determine the average density of particles expected at each detector for a cosmic ray of a particular primary energy. One advantage is that and this code is much quicker to run and also, for this project, determining the average expected particle density at the detector stations is more useful compared to a single realisation as would be obtained from a single CORSIKA run. The simulation code used in this thesis will be explained in more detail in chapter 4.

3 IceCube and IceTop

IceCube is the world's largest neutrino telescope and is situated at the South Pole. It consists of a surface air shower array IceTop [6], and an in-ice Cherenkov detector (IceCube) with a densely instrument core called DeepCore.

The IceTop air shower array is a multi-purpose detector with many scientific goals. The primary purpose of the array is to study cosmic rays. In this thesis we are interested in IceTop's ability to act as a veto against the muons from cosmic ray induced extensive air showers. If there is a candidate neutrino event in IceCube (inice event), IceTop can be interrogated for surface activity characteristic of cosmic-ray induced background. In this way any muons produced by air showers which also register in IceTop should be vetoed.

3.1 IceCube Neutrino Detector

The IceCube neutrino detector 3.1 was completed in 2010. The detector consist of 86 strings (or cables), each equipped with 60 optical sensors referred to as Digital Optical Modules or DOMs. Altogether there are 5,160 DOMs are deployed in the ice. The DOMs are deployed between the depths of 1450m and 2450m below the surface at the South Pole. The instrumented volume of IceCube is a cubic kilometer. The string spacing of 125m limits the energy threshold of IceCube neutrino detection to $\sim$ 1 TeV.

At the centre of the IceCube neutrino detector the strings have a closer spacing

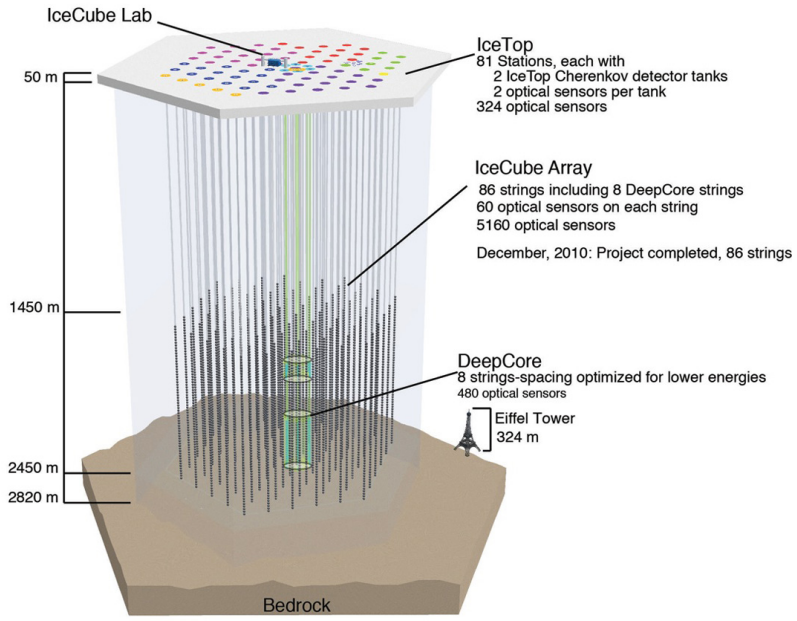

Figure 3.1: A schematic view of IceCube Neutrino Observatory. The vertical lines show 86 IceCube strings with 60 digital optical modules instrumented on each string between the depth of 1450m and 2450m. At the centre of the IceCube detector 8 strings, shown in green colour, are deployed relatively close to optimise for lower energies. This region is called DeepCore.

of between 40-70m, and the DOMs also have a closer spaccing n the strings. This denser detector is called "DeepCore" and reduces the threshold of IceCube neutrino detection to 10 GeV.

In 2013 IceCube reported 28 high-energy neutrino events found in the data collected between May 2010 and May 2012 [38]. These events are inconsistent with being background events at the 4σ level and are therefore likely to be of astrophysical origin. This discovery of cosmic neutrinos has opened the new window of astrophysics. Cosmic neutrinos, being neutral particles, provide a unique view to the most extreme environments of the universe such as black holes, neutron stars and stellar explosions.

3.2 IceTop

Low fluxes of cosmic rays at ultra-high energies make their detection only possible by measuring the Extensive Air Showers (EAS) described in the previous chapter. Through the measurement of the EAS, information pertaining to the cosmic ray energy spectrum, flux, and mass composition of the cosmic rays can be found. There are many EAS detection techniques one of them is by using the surface detectors such as the IecTop detector array, which detects the particle flux of an EAS at a particular stage of the shower development.

IceTop, shown in Figure 3.2, the surface component of the IceCube neutrino detector, is an extensive air shower detector array on the surface above the neutrino telescope [6]. It was completed in 2011 and covers 1 km^2 of area. IceTop consist of 81 stations, with average separation distance of 125 m. These stations are on top of each IceCube string. Each IceTop station has two tanks separated by 10 m. Each tank is equipped with two Digital Optical Modules (DOMs). Stations at the centre of IceTop are deployed at relatively smaller distances compared to the rest of the IceTop stations, which makes at denser array called the InFill array. The InFill array is made to lower the energy threshold of IceTop to around 100 TeV and to study the properties of low energy cosmic ray air showers. [39].

IceTop is situated at 2835 m above the sea level which coincide with an atmospheric depth of 680 gcm^{-2}. Approximately, at this atmospheric depth most of the air shower for which IceTop is sensitive, reaches to their maximum. This ideal altitude of the IceTop air shower array provides a good statistics of air shower secondary particles to study the cosmic ray air showers. IceTop is used to study energy spectrum and composition of cosmic rays between the energy range of 10^{14} and 10^{18} eV.

IceTop can also act as a coincident veto system to reduce the background events in the IceCube neutrino detector which is the focus of this thesis. High energy muons and neutrinos produced in the extensive air showers (EAS) are able to penetrate the ice and be detected by IceCube. If a signal is observed by IceCube and detected by IceTop within a specific time window, then this signal can be discarded as being atmospheric in origin.

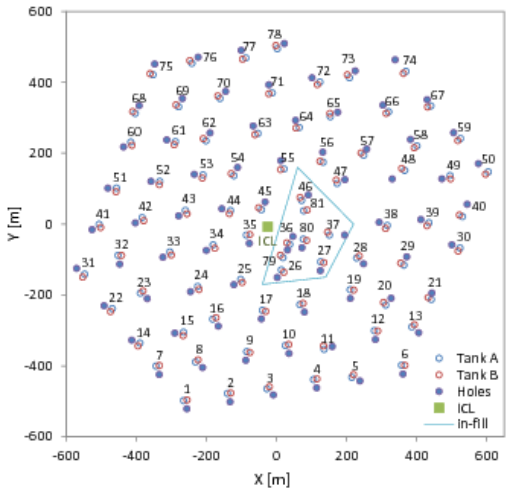

Figure 3.2: A schematic picture of IceTop air shower array. Each dot represents an IceTop tank where a pair of dots forms an IceTop station. The tanks in each station are separated by 10 m from each other and labeled as A and B. The InFill array is situated at the centre of the detector with the closer spacing between the stations. The green box represents the IceCube Laboratory which contains all the electronics to process the data.

3.2.1 IceTop Tank

Each IceTop station consist of two tanks. Two DOMs are placed, separated 58 cm between their centres, at the top of the ice in each IceTop tank, see Fig 3.3. IceTop tanks are made of 6 mm thick, 1.1 m high black, cross-linked polyethylene with an inner diameter of 1.82 m. Each tank is filled with ice to a height of 0.90 m. The space between the ice surface and the lid of the tank is filled with a material called perlite for thermal insulation. Most of the IceTop tanks have a diffusely reflective white liner made of Zirconium dioxide powder to improve the light yield at the photomultiplier.

The two DOMs inside each IceTop tank work at two different gains, high gain: 5×10^6 ; low gain: 10^5, in order to cover the large dynamic range of possible energy deposits by air shower particles. Low gain DOMs can measure high energy deposits in a region where high DOMs would have been saturated to increase the linear dynamic range of the tanks.

IceTop tanks function the same way as the water tanks of the Pierre Auger Ob-

servatory [40] and the Haverah Park experiment [41].

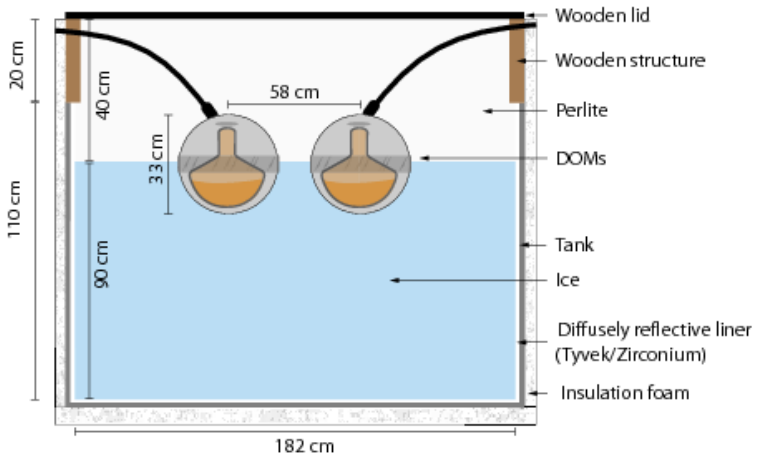

Figure 3.3: The cross section view of IceTop tank. The figure is taken from [6].

3.2.2 Digital Optical Module (DOM)

The digital optical module (DOM) [42] is a data acquisition unit for the IceCube neutrino detector. It is a basic light sensor that is used to detect Cherenkov light produced by charged particles in ice. Each DOM contains a 25 cm diameter PMT (Hamamatsu R7081-02), a high voltage (HV) power generator, the DOM Main Board (MB), a signal delay board, and a 13 mm thick glass sphere [42] [43]. In addition, each DOM has an LED flasher board which is used for calibration and to study the optical properties of the ice. These LEDs are only used for inice DOMs and not for IceTop DOMs. The DOM main board contains the electronic which is used to amplify and digitize the signals from the PMT. The PMT is protected from Earth's magnetic field by a mu-metal grid. A schematic view of the IceCube's digital optical sensor is shown in Figure 3.4.

The assembled DOM is filled with dry nitrogen to a pressure of approximately half of the atmospheric pressure. The FPGA (Field Programmable Gate Array), on the main board of the DOM, is responsible for data taking, triggering, digitization and the communication between the DOM and the IceCube Lab on the surface of the ice.

IceTop DOMs have the same hardware as the DOMs in the IceCube detector but with some different characteristics of the data acquisition system due to different environmental conditions and physical requirements [6]. The IceTop DOMs are

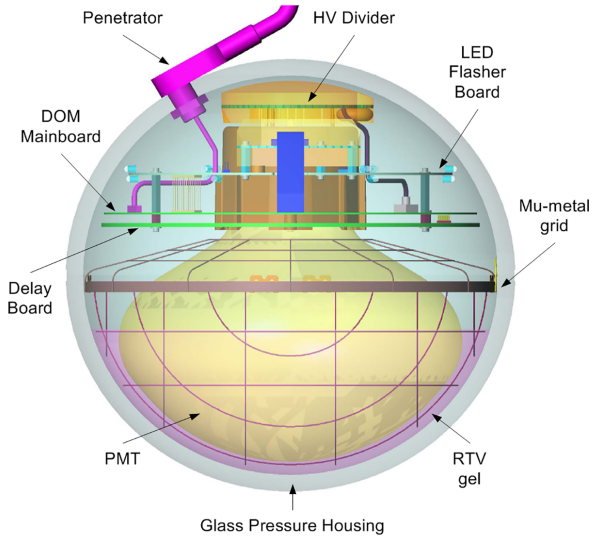

Figure 3.4: IceCube neutrino detector's light sensor and data acquisition unit (DOM).Taken from [42]

numbered from 61 to 64 in each station, where 61 and 63 are high gain (HG) DOMs and 62 and 64 are low gain (LG) DOMs, as shwon in Fig 3.5. Whereas, the IceCube DOMs are numbered from 1 to 60 from top to bottom of the IceCube string.

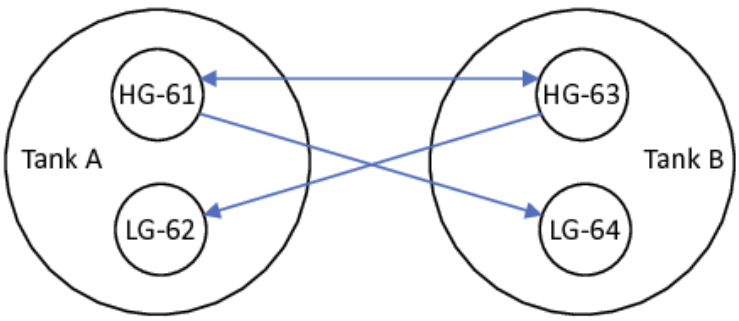

Figure 3.5: The schematic view of IceTop DOM numbering in each station. The DOMs labeled as 61 and 63 are high gain DOMs and 62 and 64 are low gain DOMs.

3.3 IceCube method of detecting neutrinos

IceCube detects neutrinos when they interact in the instrumented ice or surrounding ice and bed-rock. When a neutrino interacts with a nucleus, relativistic charged particles are created which travel faster than the local speed of light and therefore emit Cherenkov light. IceCube detects the optical Cherenkov light emitted by these charged particles. Events are separated by the pattern of light produced in the detector which itself depends on the neutrino flavour and the type of interaction as will now be discussed.

Neutrinos interact with nucleons via either the charged current or neutral current interaction. If the neutrino interacts by the charge current interaction its corresponding charged partner is produced. That is, an interacting electron neutrino produces an electron, a muon neutrino a muon and a tau neutrino, a tauon. An electron travels only a small distance in the ice before it initiates a cascade of particles. This cascade is referred to as an electromagnetic cascade as it is started by an electron. A muon, in contrast, can travel large distance through the ice. If enough energy is transferred to this muon then it can traverse across the entire IceCube detector. In all neutrino interactions, charged current and neutral current, the energy transferred to the interacting nucleus spawns a hadronic cascade of particles. In neutral current interactions, neutrino are produced which escape the detector without producing any light and the only signature from neutral current interaction is from the hadronic cascade.

The patterns of light seen in the detector are different for a cascade and a long-range particle. As the cascades typically have a length less than 10m, they appear as essentially a point-source of light. Although the Cherenkov light emitted by the cascade light is emitted in a direction related to the direction of the original neutrino, scattering in the ice means that the light loses this directional information after a few scattering lengths. This means that light emitted from the cascade has a spherical looking pattern as shown in Figure 3.6a. The pattern of light from a long-range particle like a muon is shown in Figure 3.6b. As the muon emits lights over its entire path, the direction of the muon, and therefore the original neutrino, is more easily determined.

Cascades are produced by the charged current interaction of the electron neutrino and the neutral current interaction of all three flavours of neutrinos. Whereas, track like events are initiated when a muon neutrino, and most tau neutrinos, interact via the charged current interaction. In a particular energy range of tau neutrinos the double-bang signature is expected as shown in Fig 3.6c. This occurs

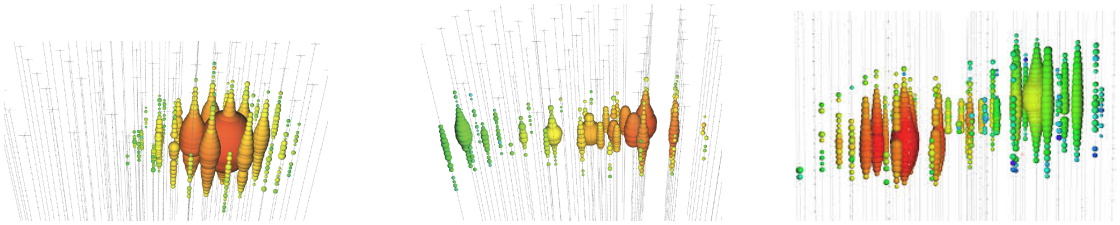

(a) Cascade event (b) Track like event (c) Double bang event

Figure 3.6: Light patterns of neutrino interactions in IceCube, caused by different neutrino flavours. The size and the colour of each circle represents the measured charge and time by the corresponding DOM.

when a tau neutrino undergoes a charged current interaction. The first ''bang" is the light produced by the hadronic. The tau lepton travels some distance, emitting Cherenkov light, and then if it decays with the detector, the decay products initiate another shower of particles which is the second 'bang". This double-bang signature only occurs if the tau particle has sufficient energy so the time dilated decay time of the tau particle means that the tau travels a sufficient distance so that two 'bangs" can be visibly separated, and not so much energy that the tau particle leaves the detector before decaying. The favourable energy range is in the PeV range. The double bang signature has not been seen in IceCube.

3.4 IceCube analysis strategies

The data collected by the IceCube neutrino detector at the South Pole is dominated by a large amount of muon background, created not by neutrinos from astrophysical sources but by cosmic rays impacting the atmosphere above the detector. This background is at a level of at least a factor of 10^6 above the signal events. A series of cuts based on different variables are made on the experimental data to reduce (and ideally remove) the background. These cuts remove some portion of the signal as well, because there are no ideal variables which uniquely separate background from signal events. Instead the variables' values serve as an indication of whether the event is more likely to be signal than background. Typically there are different analysis strategies which concentrate on a particular difference between signal and background, and on a particular type of event. For example some analysis strategies concentrate on cascade like events and others on track like events. This is because the strategies for removing background can usually be better refined if one event signature is focused on.

The first stage of filtering for all analysis types is done at the Pole and the different Pole filters create corresponding data samples which can overlap. Further analysis is done by applying reconstruction routines and cuts on one or more of these data samples.

This thesis is particularly concerned with cascade analyses. Although track events have better direction reconstruction, cascade events have better energy reconstruction, as all of the neutrino energy is transferred to charge particles which stay within the detector volume, as compared to muons which deposit their energy over the entire track length and often the muon enters and/or leaves the detector.

The cascade channel aims to select the events which are cascade like (see Figure 3.6a). For example, the pole filtering for the cascades usually consists of two cuts placed on variables called the line-fit velocity and the tensor of inertia eigenvalue ratio. The line-fit velocity variable is a quantity, which differentiates between a cascade event and a muon event on the basis of the different characteristics of the speed of light pattern passing through the IceCube detector volume. For muon events the source of light moves through the detector at the speed approaching c and so expected to have larger values of line-fit velocity. In contrast, as mentioned in the previous chapter, the cascade can be thought of as a stationary source of light due to its small spatial extent and time duration. For this reason the cascade events are supposed to have a line-fit velocity close to zero. The second variable is called the Tensor of Inertia Eigenvalue Ratio; it deals with distribution of light of an event along the three principal axes in the detector (the name of the variable using the analogy of a light distribution with a mass distribution). The eigenvalue ratio is the ratio of the lowest eigenvalue to the sum of all three eigenvalues. For a perfectly spherical event the eigenvalue ratio would be 1/3 because all three eigenvalues would be equal, while a track-like event is elongated and has an eigenvalue ratio close to zero. In the first stages of the filter levels the aim is to reduce the experimental data to a level where more sophisticated and computationally expensive reconstruction routines can be run.

Although the main aim of this thesis is to investigate how an IceTop veto can be used in a cascade analysis, in one of the studies performed it was most useful to use data with a good angular resolution. The most suitable stream of data for this study is the one containing high-energy events. The data stream used is called the Extremely High Energy (EHE) event sample and consists of events which triggered the in-ice detector with a charge at least 1000 photoelectrons (PE). Most of these events will be muon background events.

3.5 IceTop Veto Strategy

There are some initiatives [44] within the IceCube collaboration to use IceTop as a veto to distinguish astrophysical neutrino events from events initiated by atmospheric neutrinos and muons. The most advanced studies have been done by Delia Tosi [45] [46]. This study is mostly concerned about the muon neutrinos that interact and start a track in the volume between IceTop and IceCube and get lost in the background of down going muons. The analysis is particularly interested in down-going bright events which cross both IceCube and IceTop array, with an impact point [1] inside the boundaries of IceTop by at least 75 m.

The project described in this thesis is particularly focused on investigating the implementation of an IceTop veto for the cascade channel. The veto will only be used once many cascade cuts have already been made. The envisaged purpose of the IceTop veto is to allow the relaxation of other cut criteria in a way which will allow more signal to be retained.

[1] The intersection point of the extrapolated direction of the event with the IceTop surface

4 Simulation of Cosmic Ray Air Showers on IceTop

This chapter describes the code which can be used to simulate an extensive air shower impacting on the IceTop air shower array detectors. An original study performed to compare the results of the code with real data is also described.

4.1 Simulation Code Approach

The aim of the simulation code is to determine the IceTop response to an incident cosmic ray with a specified energy, zenith angle and surface impact point. The code takes a proton as the primary particle and combines the parametrised particle distributions given in chapter 2 to determine the the muon and electron density at various points on the detector surface. The procedure was written into a python script by Sebastian Euler [47] and was extended by myself in various places. In particular, the calculation of the energy of the primary cosmic ray particle and shower core interaction point with the ice surface were included as part of this project. The code is included in Appendix A.

Generally the code performs the following steps:

- Create an array of detectors
- Take the InIce event[1] and calculate the energy of the primary cosmic ray particle and shower core interaction point with ice surface.

[1]The event which has its vertex position inside the IceCube detector.

- Simulate the cosmic ray air shower with given primary cosmic ray energy, zenith and azimuth angle.
- Calculate the longitudinal and lateral development of the shower at each detector.
- Calculate the probability of detection occurring (this step can be omitted with the muon and electron density outputted rather than the detection probability).

Some of the key aspects which are calculated within the code are described below.

4.1.1 Array geometry

In the code the detector array can be constructed using two methods: using a square linear mesh of detector or from a list of detector coordinates. There are two detector coordinate options 'IceTop' or 'IceVeto'. If either of these are selected the code reads a file containing IceTop or IceVeto detector coordinates and produces the respective air shower array detector. Air shower array geometries provided by the code are shown in Fig 4.1. This project is particularly concerned about the IceTop air shower detector array. The 'IceVeto' array is a proposed future extended array.

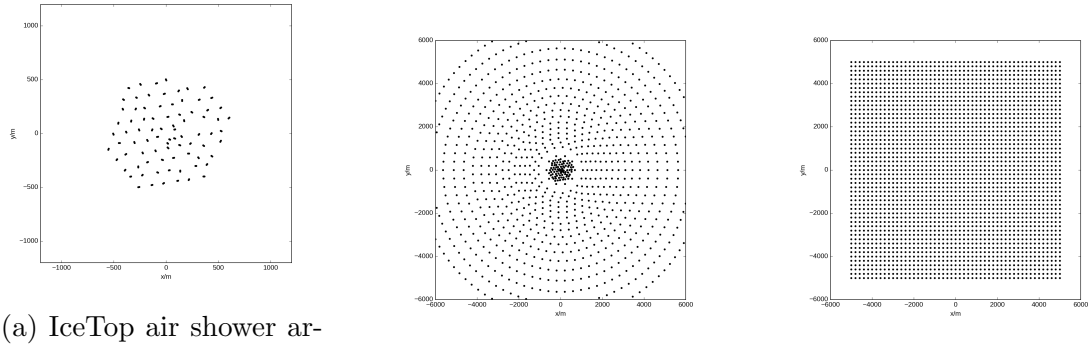

(a) IceTop air shower array

(b) IceVeto

(c) Linear Array

Figure 4.1: Different detector array geometries. (a) Shows IceTop geometry. Here one pair of two dots represents one IceTop station and each dot is a symbol of an IceTop tank. (b) The suggested extension of current IceTop air shower array, which is known as IceVeto. (c) is a linear array of detectors.

4.1.2 Effective Area

The particles produced in an inclined shower to the detector plane do not see the same cross-sectional area of a detector as the particles produced in a perpendicular shower. This effect is also included in the code, in order to estimate the number of particles a detector is expected to see.

By assuming that each detector is a cube in shape with cross-sectional area a, and thickness z. Then the width of the detector can be given as:

$$w = \sqrt{a}. \tag{4.1}$$

A baseline can be derived as:

$$b = \sqrt{z^2 + w^2}. \tag{4.2}$$

The effective area of the detector is:

$$a_{eff} = b\cos(\alpha)w. \tag{4.3}$$

here α is defined as:

$$\alpha = \arccos(D_\theta) - \arcsin(\frac{z}{b}). \tag{4.4}$$

4.1.3 Distance calculation

In order to be able to evaluate the particle distribution functions the distance between each detector and the shower core interaction point, on the same plane, needs to be calculated. It can be written in vector form as shown below:

$$\mathbf{P} = \begin{pmatrix} \Delta x \\ \Delta y \\ \Delta z \end{pmatrix}$$

Given $(x, y, 0)$ is the position of each detector whereas $(x_{\text{shower}}, y_{\text{shower}}, 0)$ is the shower core interaction point with the ice surface, the above equation can be modified as:

$$\mathbf{P} = \begin{pmatrix} x - x_{\text{shower}} \\ y - y_{\text{shower}} \\ 0 \end{pmatrix} \tag{4.5}$$

The unit direction vector of the shower core axis can be expressed in Cartesian coordinates as:

$$\mathbf{D} = \begin{pmatrix} \sin(\arccos(D_\theta))\cos(D_\phi) \\ \sin(\arccos(D_\theta))\sin(D_\phi) \\ D_\theta \end{pmatrix}. \tag{4.6}$$

Here D_θ and D_ϕ are the zenith and azimuth angles of the shower, respectively. Using the equations 4.5 and 4.6, the lateral distance between the shower core and each detector can be calculated by taking the norm of the cross product of $\mathbf{P}$ and $\mathbf{D}$,

$$r = \mid \mathbf{P} \times \mathbf{D} \mid . \tag{4.7}$$

4.1.4 Lateral and Longitudinal Shower Development

The parametrisations described in chapter 2 can be used to determine the muon and electron density.

The first step is to use the equations 2.15, 2.18 and 2.19 to determine the position of the maximum shower development and the number of electrons and muons produced at this maximum development of the shower.

The number of electrons and muons produced at the stage of shower detection is calculated by using equations 2.20 and 2.21, respectively.

For the lateral development of the shower, the density of the electrons and muons was calculated using equations 2.22 and 2.23, respectively. Here the density of the particles can be taken as the expected cumulative number of particles per unit area after the shower event has completely finished.

4.1.5 Detection mechanism

The parametrisation code can be used in two different modes:

Mode 1: Code can be used to estimate the average electron and muon density at positions on the surface due to an air shower. This mode for running the code is not actually a Monte Carlo simulation but purely evaluating the various distribution functions for appropriate column density.

Mode 2: Code can be used determine number of hit tanks. This mode is a Monte Carlo which uses the average electron and muon densities and a random number in a Poisson trigger expression to decide whether a tank records a hit or not.

Poisson Trigger

Poisson statistics is commonly used to estimate the probability of making k detections. The detector array get triggered when the number of detected daughter particles produced in the shower exceeds a threshold value, τ.

$$P(k) = \frac{\lambda^k e^{-\lambda}}{k!} \tag{4.8}$$

The mean number of particles expected at a detector with an effective area α and particle density ρ, is given by ($\lambda = \alpha\rho$). So the above equation can be written as:

$$P(k) = \frac{(\alpha\rho)^k e^{-\alpha\rho}}{k!}. \tag{4.9}$$

The probability of getting at least one detection is given as:

$$P(1 \text{ or more}) = 1 - P(0 \text{ detections}) = 1 - e^{-\alpha\rho}. \tag{4.10}$$

A random number ($P_{\text{rand}} = \text{Rand}(0, 1)$) is generated and compared to the cumulative distribution of Poisson probabilities in order to decide whether the particle is detected by the detector or not. The particle is detected if:

$$P_{rand} \leq P(1 \text{ or more}). \tag{4.11}$$

Shower Detection

The above process is repeated for all the detectors in the detector array to check if the particle is detected or not. If the number of triggered detectors is greater than or equal to the threshold values τ, then the shower has been detected by the array. For this project τ is set to 1.

4.1.6 Output response from the code

The code takes the energy E_{prim} of the cosmic ray primary particle, zenith angle θ, azimuth angle ϕ and, the interaction point of the shower core at the ice surface as an input and returns the number of muon and electron hits for a particular at particular locations. Figure 4.2 shows the example response for an extensive air shower from the code. The shower was created at an arbitrary values of E_{prim}, θ and, ϕ.

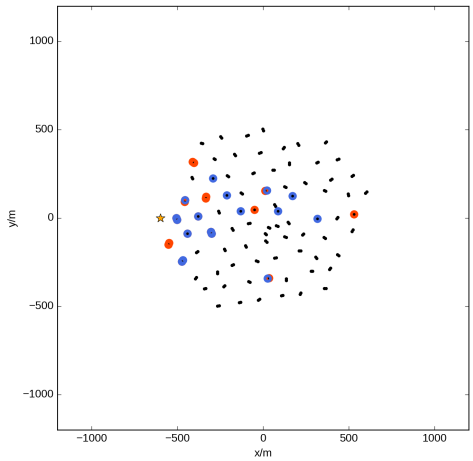

Figure 4.2: The output response of parametrisation based simulation. The blue and orange dots represent the muon and electron hits, respectively. The yellow star shows the interaction point of the shower core with the ice surface.

4.2 Comparison of the Parametrisation code with CORSIKA

Sebastian Euler performed a cross-check with CORSIKA [48]. The output from the parametrisation based simulation code, described above was compared with outuput from CORSIKA simulations using the same detector array geometries. An excellent agreement is seen between CORSIKA and parametrisation based simulation, see figure 4.3. The two plots in figure 4.3 display the probability that a cosmic ray event will pass IceTop without detection and show that low-energy events are likely to pass without detection while high-high energy events are likely to be detected (have a low probability of non-detection). The two plots show two different zenith angle intervals for the incident cosmic ray. Both plots show that the shaded prediction from the parametrisation code is in good agreement with the CORSIKA simulation results.

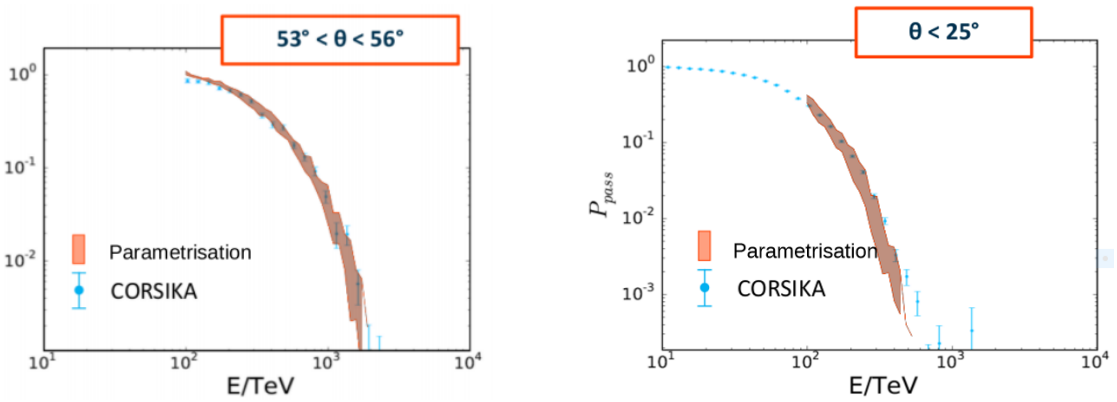

(a) (b)

Figure 4.3: Comparison of parametrisation base simulation with CORSIKA.

4.3 Comparison of the parametrisation code output with data

In this study we wanted to investigate how the output from the parametrisation code compares with data events detected by IceCube. This study had two aims, the first is to simply make the code-data comparison and the second is to use this comparison to inform how the IceTop veto logic might be applied. With regard to the second aim, one possibility for using the IceTop event information is to take neutrino candidate events detected by the IceCube inice array, and use the inice information to deduce the likely IceTop hits if the candidate event was actually muon background rather than a neutrino event, and compare this prediction with detected IceTop hits. The parametrisation code can be used to predict number of IceTop hits for a cosmic ray event if the cosmic ray zenith angle, energy and surface intercept are known. In this study a sample of IceCube events which should be essentially all background events was used. The inice event information (light distribution) for each event in the sample was used to predict the cosmic ray zenith angle, energy and surface intercept of the cosmic ray source. This information was piped into the simulation code and the IceTop response was predicted. The predicted IceTop response was compared with the actual charge/hits recorded in the IceTop array.

The event sample used was the Extremely High Energy (EHE) sample as these events have a good angular reconstruction meaning the zenith angle and related surface intercept should be determined reasonably accurately. Only those InIce events were selected which are reconstructed as downgoing events (events which

originate from above the detector).

The code takes the reconstructed position and angles (zenith and azimuth) of the inice event and calculates the shower core position at IceTop surface using the following equations.

$$s = \frac{(1950 - P(z)_{inIce})}{\mathbf{v}_z} \tag{4.12}$$

$$P_{surface} = P(event)_{inIce} + s * \mathbf{v}_{(x,y,z)} \tag{4.13}$$

Here the terms $P(z)_{inIce}$, $\mathbf{v}_z$, $P_{surface}$, $P(event)_{inIce}$, and $\mathbf{v}_{(x,y,z)}$ are the z inIce position of the event, z direction vector, shower core position at the ice surface, in-ice position of the in-ice event, and the x, y, z direction vector, respectively. The coordinate system is that used for IceCube which has the origin in the centre of the IceCube inice array. The number 1950 is the z position of the ice surface.

4.3.1 Primary energy calculation for in-ice events

The most uncertain input to be determined is the primary energy of the cosmic ray. Firstly it is not fundamentally possible to derive a one to one relationship between the energy of the particles in the ice and the energy of the primary particle because of the quantum nature of the particle interactions involved. Secondly there are uncertainties involved in determining the energy of the particles from the amount and pattern of Cherenkov light detected. The IceCube collaboration use a quantity called MuEx which is derived from the amount and pattern of detected light and assuming the light has been produced by muons, is related to the energy of the muons.

Figure 4.4 shows a plot of MuEx versus primary particle energy[2] produced using CORSIKA simulations and tracking the particle shower from the primary cosmic ray interaction in the atmosphere into the ice and simulating the detector response. This CORSIKA simulation was subjected to the same filtering process as the EHE data sample which is used to make the comparison between data and the code output. As the plot is made from simulated data the energy of the primary particle is known. The plot shows that, as expected there is not a one-to-one

[2]This plot was produced by Hadis Bagherpour, another graduated student in the IceCube group at the University of Canterbury

relationship between the primary particle energy and the MuEx value derived; a given MuEx value result from a spread of primary particle energies as can be seen from the spread in blue shading. The median primary energy is shown in red and the first and second standard deviations are shown by the dashed lines. It can be seen that for a given MuEx 90% of primary particle energies lies a reasonably narrow range.

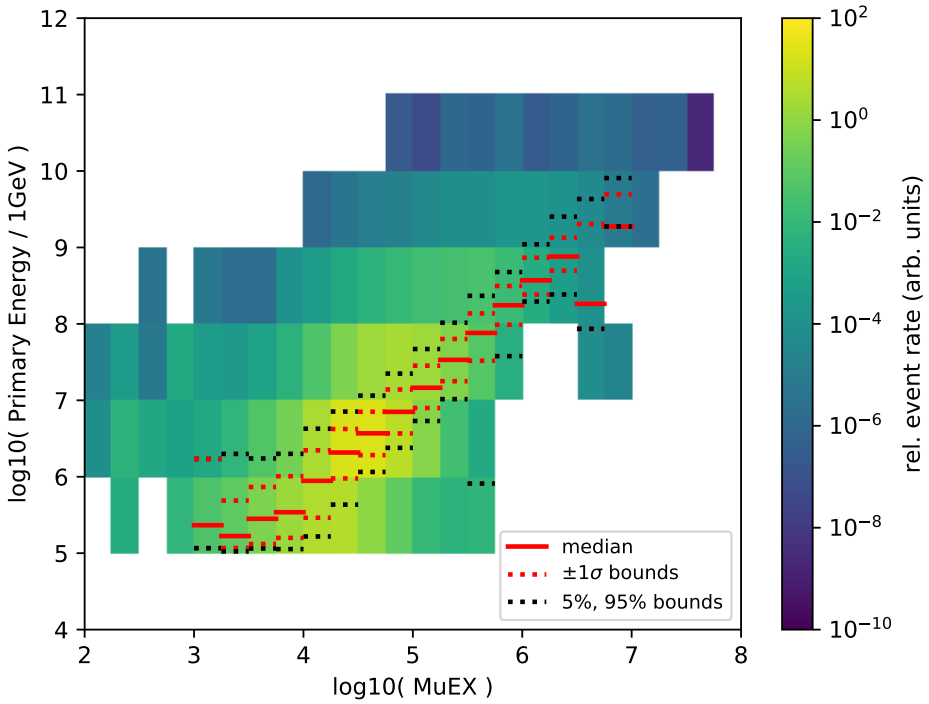

Figure 4.4: MuEx and primary energy relationship. The red solid line represents the median energy of the primary particle.

4.3.2 Results

Figures 4.6 to 4.8 are scatter plots which show the results of the comparison between the simulation code output and the IceTop hits for the EHE data sample. The vertical axis is the simulation code output while the horizontal axis is information extracted from the data sample.

To produce the vertical axis code value for a given event, the inice light distri-

bution information was used to derive the zenith angle and MuEx information using IceCube reconstruction software [3]. The zenith angle, and the first hit DOM information was used with equation 4.13 to obtain the surface intercept. A tabulated version of figure 4.4 was used to obtain a primary particle energy value from the MuEx value for the event. The median energy points on figure 4.4 were used. In this way we obtained the three inputs required for the simulation code and could use the simulation code to predict the expected hits on IceTop. We used the simulation code to give the total electron and muon density across all of the IceTop stations, taking the muon and electron density and mulitplying by the area of tanks to obtain the total predicted charge (plot (a) in each of the figures). We also used the code in the Poisson probability mode to obtain the number of expected hits (plot (b) in each of the figures).

To produce the horizontal axis data value, for each event, the IceTop data[4] was counted in a time-window of -500 ns to +800 ns relative to the inice event time. The motivation for this time window range is discussed in the section 5.4 of the next chapter. Two experimental data quantities were derived: the total charge recorded on the PMTs (for plot (a) in each of the figures) and the total number of station hits (for plot (b) in each of the figures).

Figures 4.5 and 4.6 show the code output data comparison with muon and electron density (or hits in (b) panels) combined together, while figures 4.7 and 4.8 show the comparison for the muon density and electron density predictions separately. The data values are the same for each of figures 4.7 and 4.8 as it isn't possible to distinguish the IceTop hits which came from muons and those which came from electrons (the Cherenkov light detected as no distinguishing features). Figure 4.5 displays only the near vertical events (with zenith angle in the range 0° to 10°) while figure 4.6 is for more inclined events (with zenith angle in the range 30° to 40°).

Overall the comparison is reasonable especially for the more vertical events. For the more inclined events there appears to be more IceTop charge/hits than the code predicted. This was unexpected as we had anticipated that the snow cover on the IceTop tanks[5] would reduce the signal from the predicted as the attenuating effect of the snow is not included in the code. The underestimation effect may be

[3] $MuEx\_sp3\_SPEFit12EHE\_refit\_MPE$ recoparticle was used to get the deposited energy and event reconstructed direction information.

[4] $OfflineIceTopHLCTankSLCTankMerged$ pulses were used.

[5] The IceTop tanks were installed on the surface but annual snowfall in subsequent years mean they are now buried by snow. There had been a corresponding decrease in the rate of events detected by IceCube annually due to the snow cover.

due to underestimating the primary particle energy as the MuEx to primary energy conversion may not work as well for the more slanted showers. However as far as the use of IceTop as a veto is concerned is promising that there are more hits than predicted on IceTop, but it is clear that the exact number of hits predicted is not robust.

It had been anticipated that the muon hit trend might be more reliable as muons are not attenuated by snow but given the overall number of data hits was more than predicted by the code, there seems no reason to take the conservative approach of only using the muon hits as a basis for assessing IceTop's veto capabilities.

For the slanted events (above 30^0) the prediction does not match well with the observation because the time window is not useful for the slanted events, as shown in Figure 4.6.

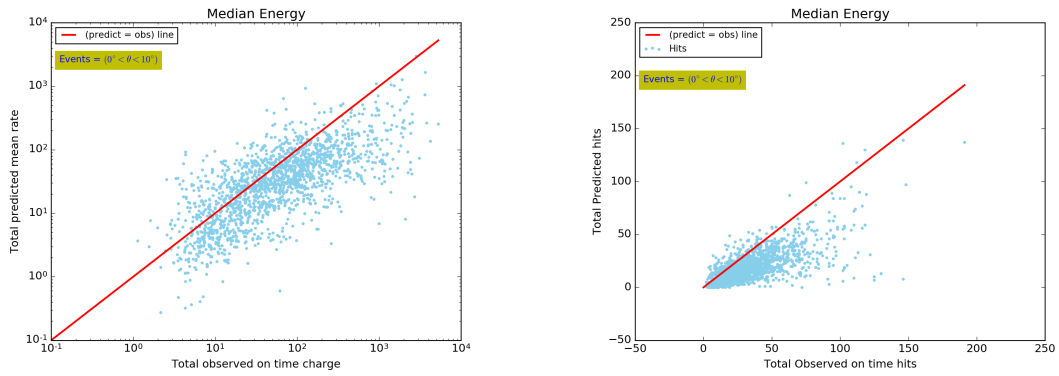

(a) (b)

Figure 4.5: Observed versus predicted total mean rate and hits for air showers incident in the zenith angle range 0° to 10°

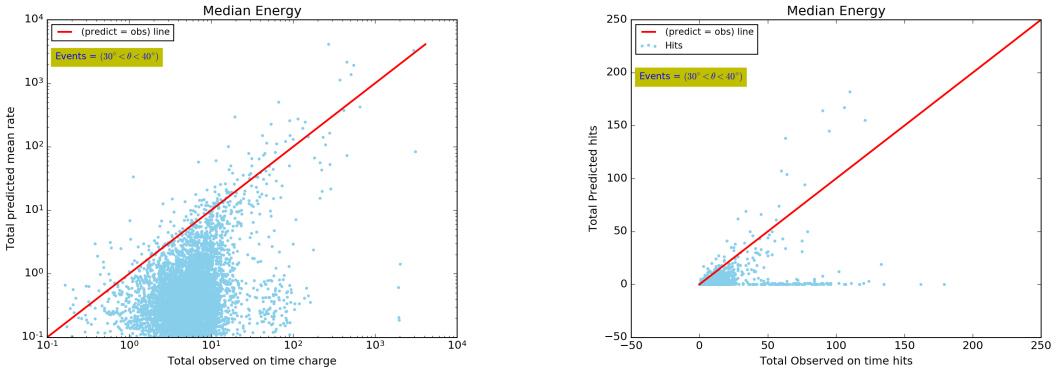

(a) (b)

Figure 4.6: Observed versus predicted total mean rate and hits for air showers incident in the zenith angle range 30° to 40°

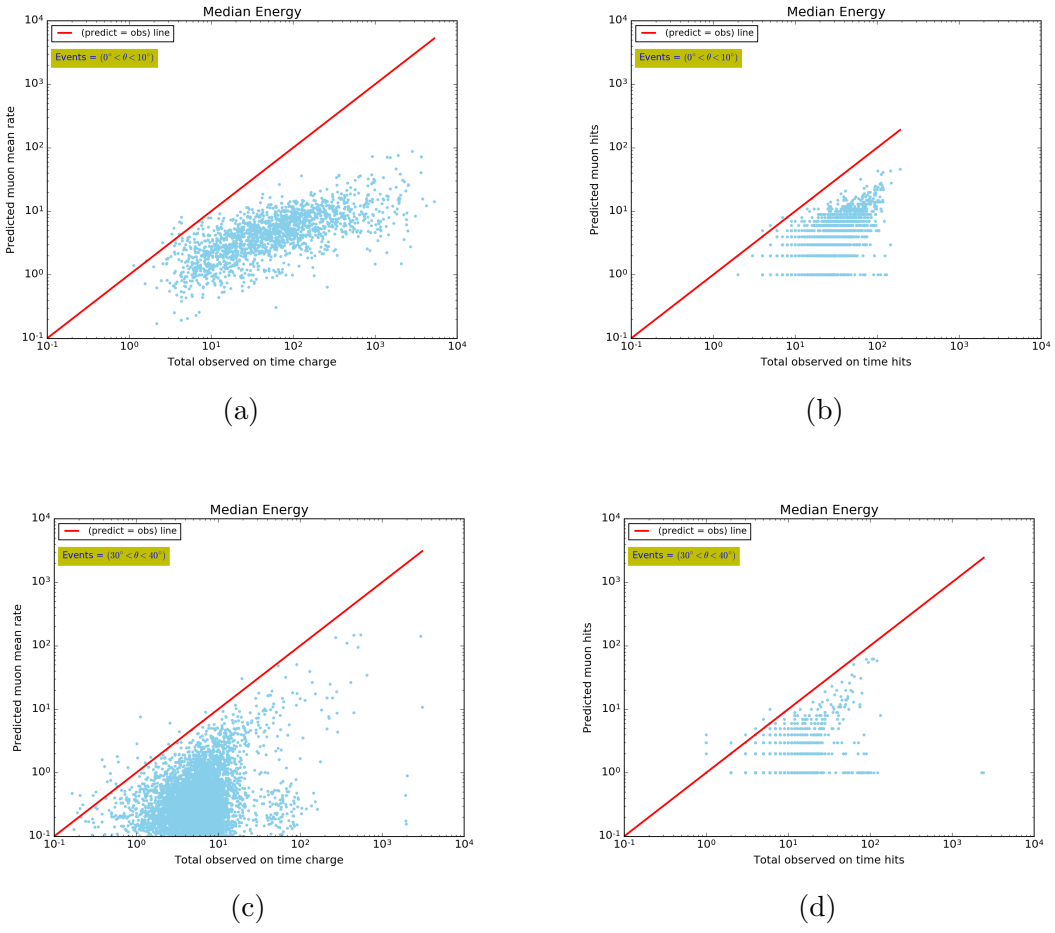

Figure 4.7: Observed versus predicted muon mean rate and hits.

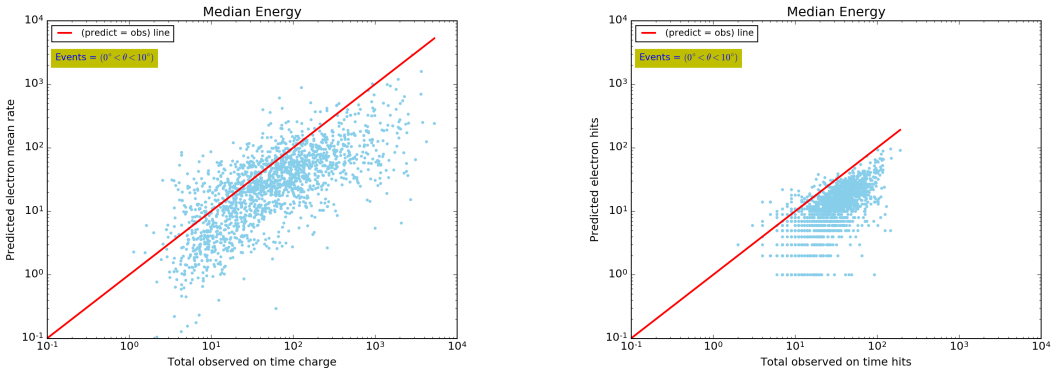

(a) (b)

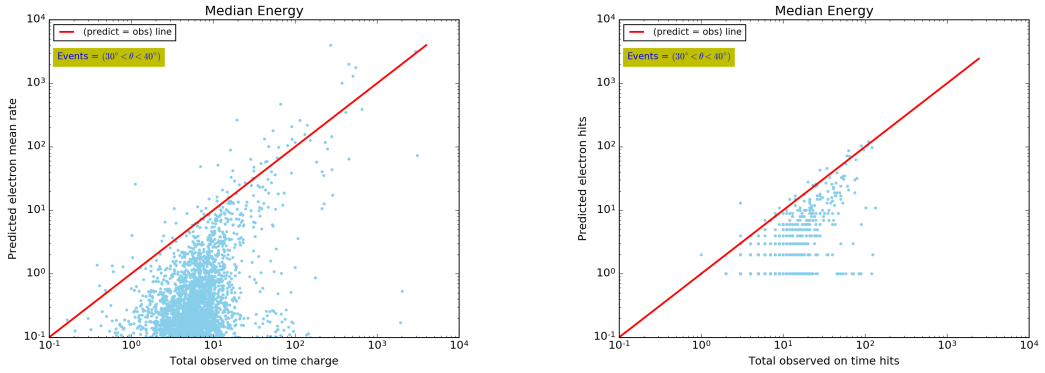

(c) (d)

Figure 4.8: Observed versus predicted electron mean rate and hits.

5 Investigating IceTop Veto possibilities

Two separate studies are presented in this chapter. The first of these uses the simulation code presented in chapter 4 to understand the parameter space over which the IceTop veto might be useful. By the term parameter space we mean the range of the cosmic ray parameters, such as the zenith angle, the primary energy and the distance of the shower core from the IceTop array. The second study looks at a suitable time-window to use for the IceTop data to define correlated hits. A defined time-window is needed to be able to associate the inice and IceTop detected signals. If this time window is too large then there is a risk that astrophysical neutrino events will be vetoed because of a chance coincidence of an unrelated air shower event with the neutrino event.

5.1 Investigation into the capability of IceTop as a veto

The probability that a cosmic ray air shower will result in hits in the IceTop array is dependent on the energy of the primary particle, the zenith angle and the distance between the shower core impact point and the IceTop array. Figure 5.1 shows a schematic view of an air shower which might result in an event being recorded in IceTop. In this figure the two panels are to make the distinction between contained and an uncontained air showers. Contained air showers are those whose impact point is within the boundary of the IceTop array. Whereas, uncontained showers have their impact point outside of the IceTop array boundary. Here the

zenith angle is defined as the angle between the shower core and its zenith. The x distance is the distance, along the x-axis, of the shower core impact point from the centre of IceTop. For example, the distance between the points A and B is the shower core impact point distance from IceTop's centre.

To understand our parameter space, we looked at how the mean number of hits varied for cosmic ray primary energy, zenith angle, and the x-distance of the shower from IceTop.

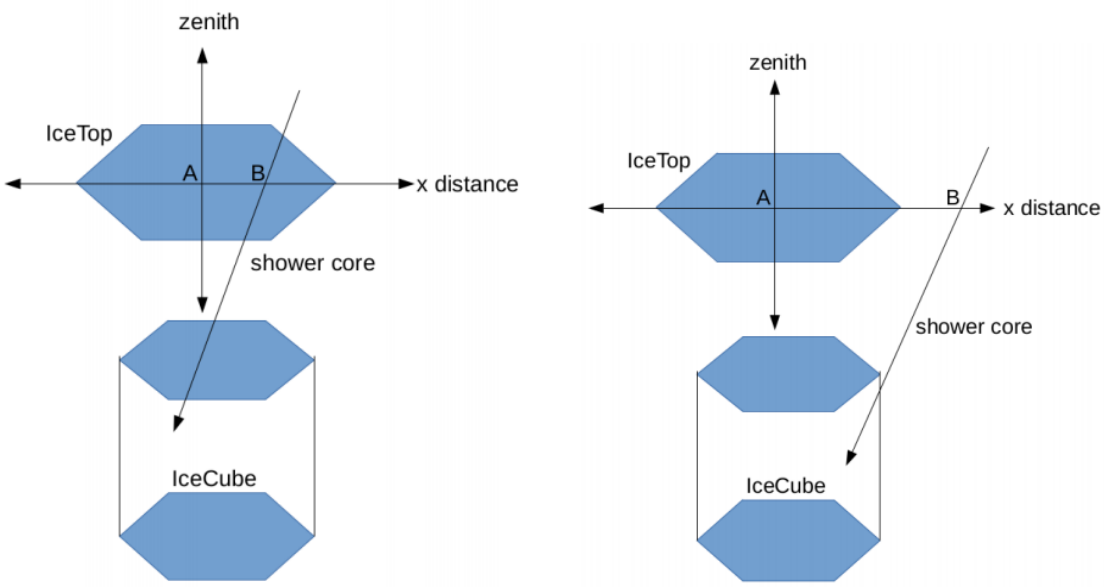

(a) IceTop-contained shower axis (b) IceTop-uncontained shower axis

Figure 5.1: Various possibilities of an air shower to enter the IceCube detector. The shower can be contained within the IceTop array boundary or outside of it.

5.1.1 Energy-zenith relationship

For each values of zenith angle and primary energy 1000 showers were simulated at an arbitrary distance from the IceTop air shower array and the mean hit rate of electrons and muons,$\sum \frac{nhits}{1000}$, was calculated. The mean number of hits are maximum for high energy downward showers, as shown in the right upper region of the Fig 5.2. This is because the number of particles created in the extensive air shower is denser near the shower core. For low energy slanted showers the relative spread is large compared to the high energy vertical showers due to the lower density of the particles far from the shower core.

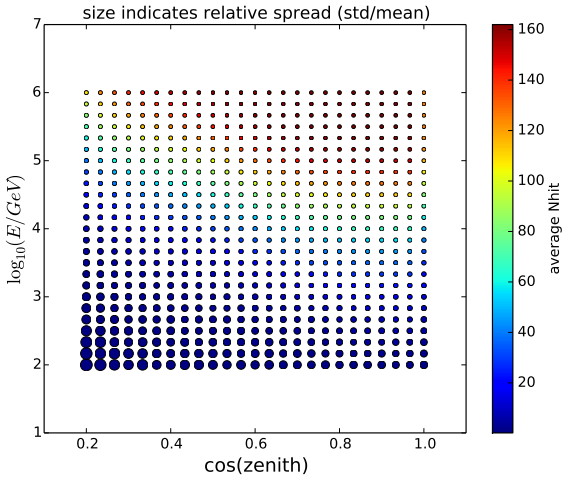

Figure 5.2: Mean number of hits, with cosmic ray primary energy on the y-axis and cos(zenith) on x-axis. The size of the circles represents the relative spread in number of hits at particular energy and zenith angle.

5.1.2 Muon hit probability as a function of distance and zenith angle

We used the Poisson rates at a fixed energy to look at the probability of seeing ≥ 1 muon hits on IceTop. The probability of getting one or more muon hits was calculated at different zenith angles and distances from the centre of the IceTop surface, see Fig 5.3. As expected, showers with small zenith angles and distances from the IceTop surface are more likely to get hits. For example, for a 100 TeV energy primary particle, one or more muon hits is only probable for showers which fall within 600m of IceTop centre. However for 100 PeV primary particle energies, almost any shower within 2km of IceTop will produce one or more muon hits.

5.2 Investigation into IceTop time window size

In this study we want to determine the time-window to use for the IceTop data within which hits would be classified as being correlated with an event detected in IceCube. If this time window is too large then there is a risk that astrophysical neutrino events will be vetoed because of a chance coincidence of an unrelated air shower event with the neutrino event. The first step is to use the geometry of the

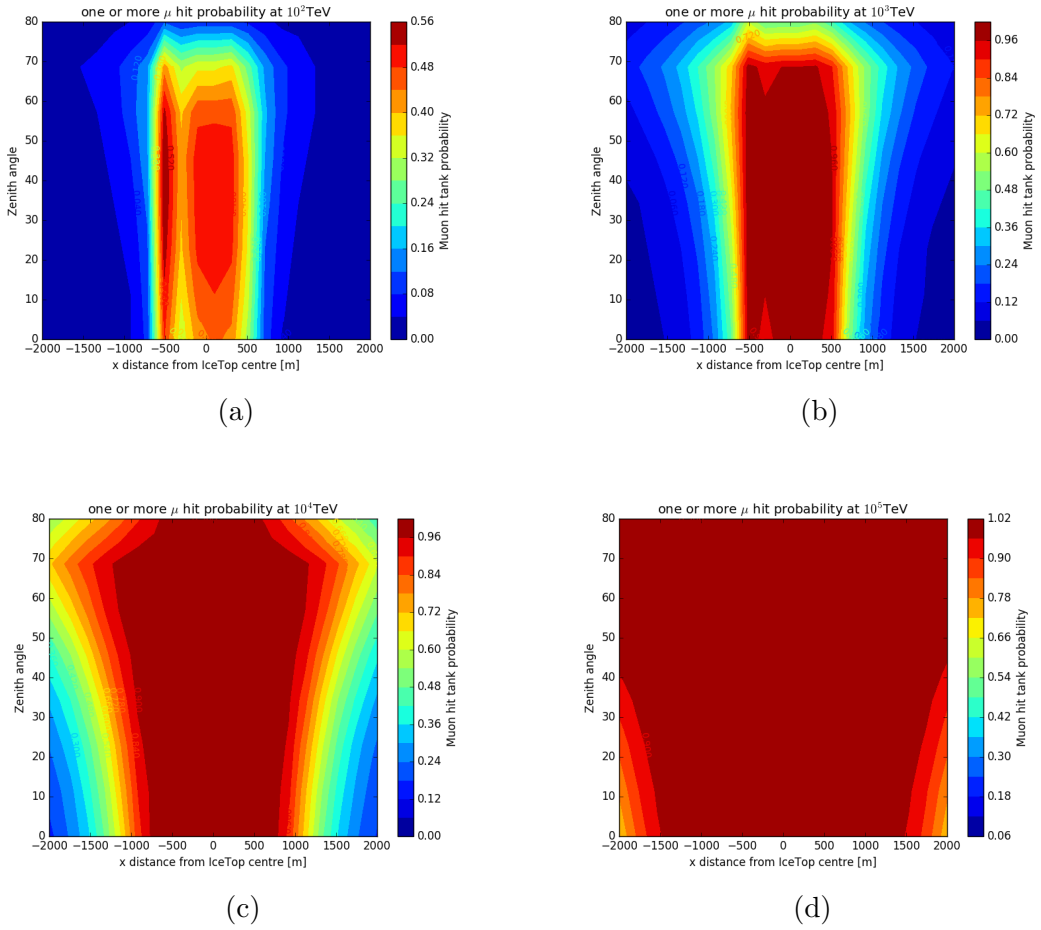

Figure 5.3: Numbers on the colour bar show the probability of getting one or more muon hits. Colours show the change in probability from high (red) to low (blue).

event detected in IceCube to determine the predicted time of impact of the shower front on IceTop relative to the timing of the event in IceCube. We then took a sample of EHE data, as used in section 4.3 and looked at the time distribution of hits around the calculated impact time to find the time window size.

5.2.1 Calculation of the front impact time on IceTop

The shower front impact time at each IceTop tank was calculated for an extrapolated shower front. The difference between the IceTop hit tank time and the expected arrival time of the shower front at that particular tank was calculated.

Figure 5.4 shows a schematic view for calculating the predicted time of the shower front at each IceTop tank. By using the inice reconstruction of the muon path with a fitted direction, position and time, the shower core impact point at the ice-surface, shown as point E in the figure, was calculated using equations 4.12 and 4.13. Then the lengths of $\overrightarrow{EC}$ and $\overrightarrow{CD}$ vectors were calculated. Here D is one of the IceTop tank. The angles between these vectors was calculated using the following relations:

$$\theta = cos^{-1}\left(\frac{\overrightarrow{EC}.\overrightarrow{CD}}{\parallel \overrightarrow{EC} \parallel . \parallel \overrightarrow{CD} \parallel}\right). \tag{5.1}$$

In $\triangle ACD$, $\angle A$, $\angle C$, and the length of $\overrightarrow{CD}$ is known. The $\triangle ACD$ was solved for $\parallel \overrightarrow{AC} \parallel$. As we know the in-ice event time (point C) the time at A, which is the expected time of the shower front at tank D, was calculated using the following equation:

$$\begin{aligned} \parallel \overrightarrow{AC} \parallel_t &= \frac{\parallel \overrightarrow{AC} \parallel}{c} \\ A_t &= E_t - \parallel \overrightarrow{AC} \parallel_t, \end{aligned} \tag{5.2}$$

.

Here, $\parallel \overrightarrow{AC} \parallel_t$ is the time light takes to travel from point A to C, E_t is the inice event time, c is the speed of light, and A_t is the time at point A.

This process is repeated for every tank on IceTop to calculate the expected shower front time at each tank. The shower front curvature is not taken into account in this calculation.

The above explained process of shower front time calculation at each IceTop tank is separate from the parametrisation-based simulation, as the code does not have any timing information in it.

5.2.2 Timing study

To study the correlated hits and time window, the inice EHE data sample was used due to the better angular resolution of the track like events. This data stream contains the events which triggered the in-ice detector with a charge at least 1000

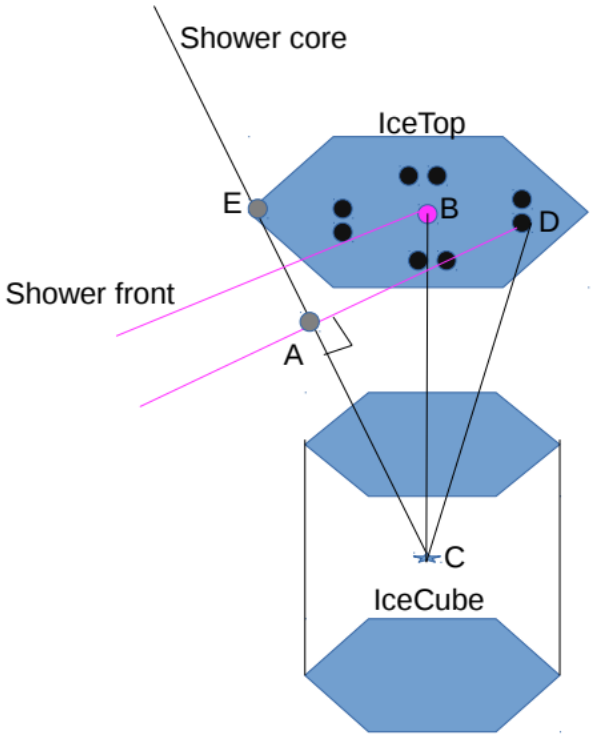

Figure 5.4: The schematic picture showing the expected shower front time calculation at each IceTop tank. The blue star represents the event recorded in IceCube and the black filled circles are the IceTop tanks. The pink circle is the IceTop centre.

photoelectrons (PE). The data was taken from 2012, specifically 2012-10-12. A total of 29048 events were in the sample.

The predicted time of the shower front at each IceTop tank, for each event, was calculated by using the procedure described in the previous section. The time difference between the actual time of a hit on any IceTop tank and the predicted time at that tank was calculated.

Figure 5.5 shows the histogram made from all of the events in the EHE sample used with the number of hits falling in each time bin shown[1] Here figure 5.5a shows the number of counts in each bin whereas in figure 5.5b the counts are weighted by the amount of charge associated with the hit. It can be seen that hits are peaked around the zero bit and that the hits associated IceCube inice event fall with -500

[1]Note that this histogram, and the others in this section, are the aggregate of many events. The number of hits per event is much smaller.

and 800 ns of that predicted using the geometrical tracing.

Some of the width of the distribution can be attributed to the air shower itself and the fact that the shower front is actually curved rather than flat as assumed in the calculation. Also any error in the zenith angle determined for the inice event will mean that the calculated shower front impact time will also be in error. A time window of -500 and 800 ns seems appropriate for well-reconstructed events such as those in the EHE sample.

The secondary peak which can be seen in figure 5.5a at around 7500ns is most likely due to after pulsing in the PMTs. This height of this peak is reduced in 5.5b suggesting that the charge associated with the hits at this time is lower than other hits. In figure

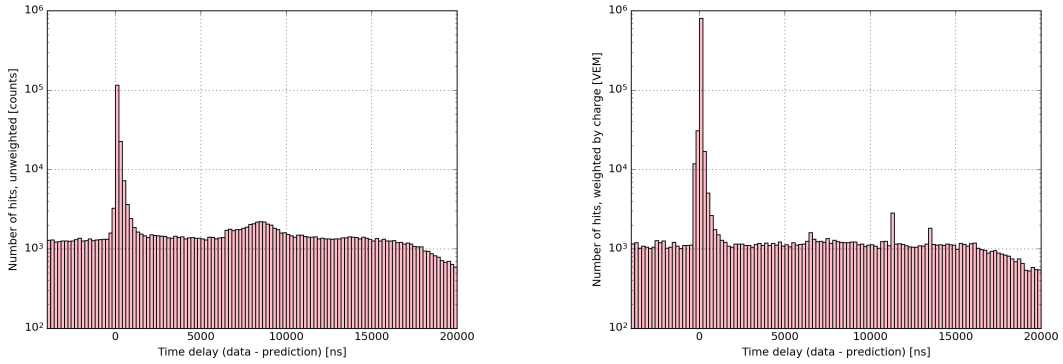

(a) (b)

Figure 5.5: Here each bin corresponds to 200 ns. Most of the hits fall within -500 and 800 nanoseconds.

Figure 5.6 shows the event histograms separated into zenith angle bands. It can be seen that the number of signal hits decrease relative to the number of background hits as the angle of the shower becomes more inclined. This is because of the fact that electrons and muons produced in the extensive air showers have lower density further from the shower core, and for these geometries a slanted event typically has a core far away from IceTop. Consequently, there are not as many hits and it is more difficult to see the hits from the event above the background rate.

For nearly vertical showers ($0^0 \leq \theta \leq 20^0$) the number of events are greater by almost a factor of 10^3 compared to the background events. For the slanted showers, for example ($30^0 \leq \theta \leq 40^0$), the event rate decrease by a factor of 10^2 compared to the event rate for nearly vertical showers. For the shower with zenith angle

above 60^0 the event rate does not seem to go above the background rate.

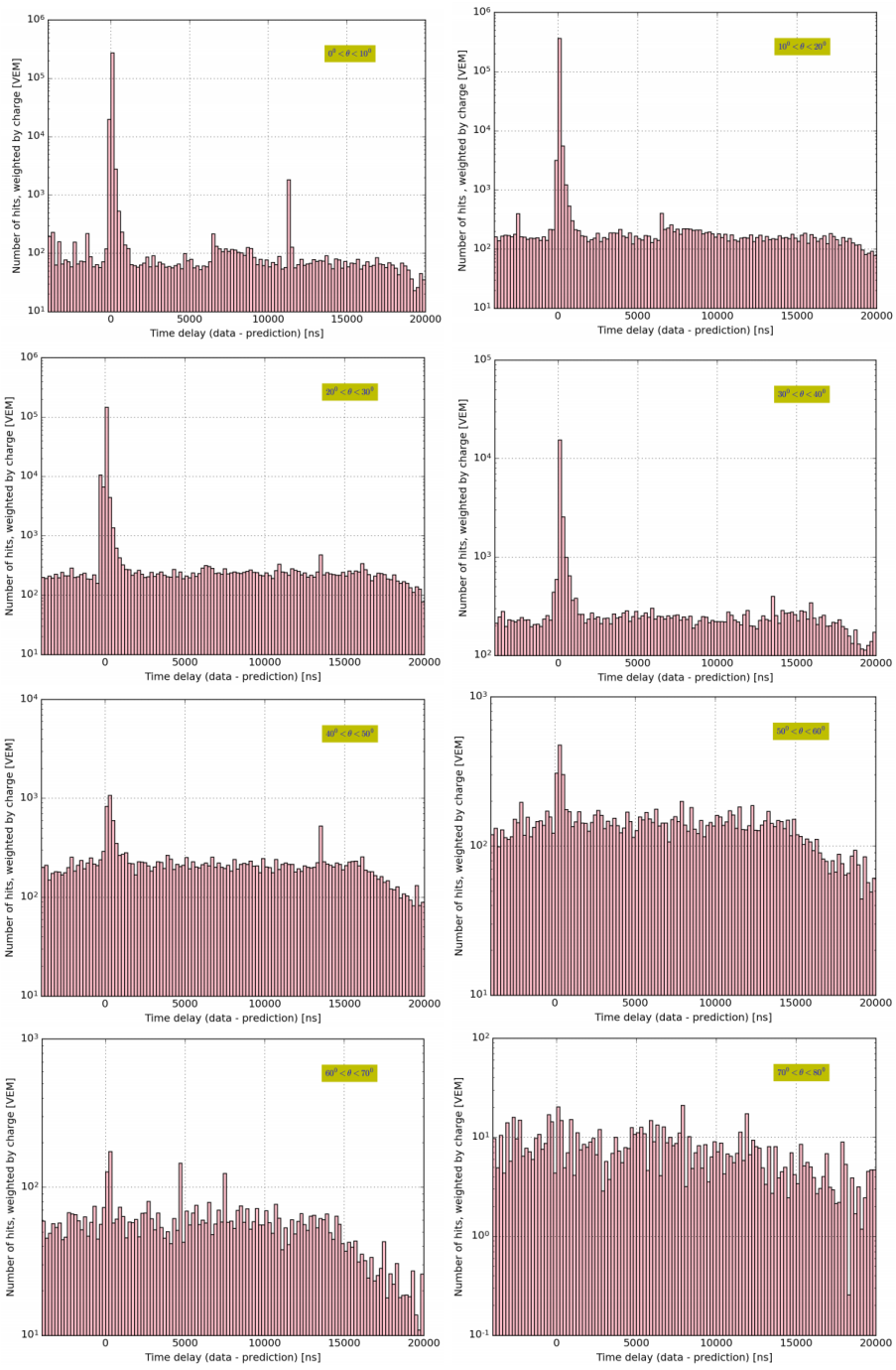

Figure 5.6: The zenith angle of the shower influences the number of hits recorded on IceTop due to the fact that inclined showers which pass through the IceCube inice detector must necessarily have their shower cores a large distance from IceTop.

6 IceTop Hits for a Partially Contained Event Sample

In this chapter an investigation is made into the likelihood and existence of IceTop hits related to an event selection which focused on cascades at the edge of IceCube's instrumental volume. This event selection was obtained by Achim Stoessl from Humboldt University [49]. IceCube cascade event analyses (see section 3.4 for a description of what is referred to as a cascade event) follow two different strategies according to where the neutrino interaction, which produces the cascade, occurs in the IceCube volume. As the nuetrino interaction point itself is unknown information on the separation is based on the first hit DOM. Achim Stoessl's analysis focused on cascades around the edges of IceCube. Such an analysis is subject to higher background but increases the detection volume by 80 % compared to analysis strategies which restrict their focus to only the inner part of the detection volume. The two approaches of *contained* and *partially contained* cascade searches are complementary and together give a larger event sample than that which results from a contained analysis alone. The higher background contamination present in the partially contained analysis motivated this study to see whether the IceTop veto could identify any of the background events remaining in the event sample.

6.1 Partially contained event sample

Figure 6.1 shows the partially contained cascade selection as a function of energy obtained by Achim Stoessl's analysis.

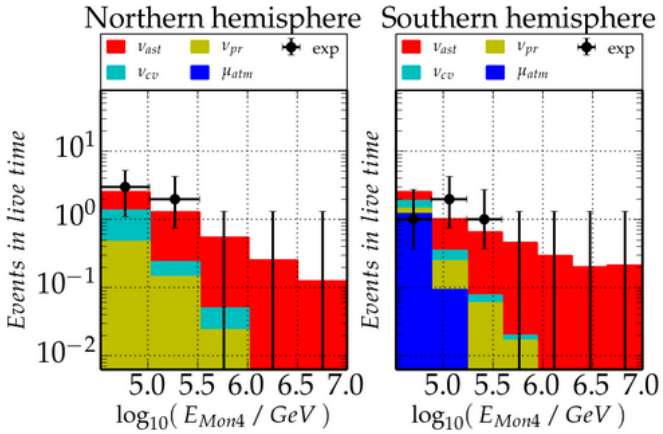

Figure 6.1: The energy spectrum of final data sample from IC79. The atmospheric muon contamination estimated to be present in the event sample is shown in blue on the right plot, from the Southern sky. The figure is taken from [49].

In the final sample of the partially contained analysis 20 events were found. These final events are shown in table 6.1. Only the events which were reconstructed as downgoing (from the Southern sky) were used for this project . Four of these events, which are marked as "*", are reconstructed as upgoing events and are not included in this study. Here $E_{\rm rec}$, $\Theta_{\rm rec}$, and $(x_{\rm rec}, y_{\rm rec}, z_{\rm rec})$ are the reconstructed energies, angles, and the positions of the events.

6.2 Investigation into the likelihood of IceTop hits

An investigation was undertaken, for each of the partially contained events to find whether we would expect for these events, given their reconstructed energies and zenith angles, to see any hits in IceTop. This investigation was performed using the simulation code described in Chapter 4 and used for my previous studies.

Showers were simulated at zenith angles, surface energy intercept distances, and energies appropriate to each particular event in the sample. As explained in section 4.3.1 the most difficult of these characteristics to deduce is the energy of the primary particle. The MuEx quantity used in section 4.3.1 is not expected to be reliable for cascade type events. Instead we use a relationship provided by our collaborator Thomas Gaisser. This relationship is discussed in the subsection below.

season	sample	run	event	E_{rec}	Θ_{rec}	x_{rec}	y_{rec}	z_{rec}
IC79*	90%	116351	5378257	54	111	2	-420	308
IC79	90%	116457	702481	174	83	497	187	-309
IC79	90%	116522	17216576	200	50	-340	85	-571
IC79	90%	116532	28124500	62	40	-617	1	-355
IC79*	90%	116698	10198436	53	247	303	-470	168
IC79	90%	116794	31146792	41	86	468	311	-460
IC79	90%	117273	15914878	93	26	227	-464	-354
IC79	90%	117721	55150085	146	87	471	-59	68
IC79*	90%	117744	54888465	34	145	44	460	-306
IC86	90%	118178	6251579	38	61	-453	-364	-501
IC86	90%	118178	66452255	89	73	-60	3	-500
IC86	10%	118420	72256529	127	59	-126	453	-145
IC86	10%	118670	58852406	300	0	638	254	-401
IC86	90%	118466	21256734	387	90	-202	-562	48
IC86	90%	118692	5825484	62	78	-424	-288	308
IC86	90%	119117	23529568	578	65	320	-482	207
IC86	90%	119507	35825553	130	78	-385	475	162
IC86	90%	119651	30979523	36	67	495	-217	-464
IC86*	90%	119736	73354228	116	100	626	145	149
IC86	90%	119962	11948966	63	50	-466	89	-532

Table 6.1: The partially contained final sample: 20 events survived all filter levels. The events marked with "*" were not included in this project.

6.2.1 Primary particle's energy calculation

The translation between the energy deposited in IceCube, E_{dep} to the cosmic ray primary energy E_{prim} was made using a relationship provided by our collaborator

Prof. Tom Gaisser from Delaware University. This energy relationship is shown in figure 6.2a and this plot is referred to as the Gaisser plot below. The deposited energy for each event in the partially contained event sample was obtained by Achim Stoessl as part of his analysis and are given in the column headed E_{rec} in table 6.1.

For the Gaisser energy relationship, on the x-axis is the primary energies of protons and iron and on the y-axis is the muon bundle deposited energy. As the relationship was only available as a graph (obtained from simulations), it was necessary to parameterise the curves shown on the graph. For this particular study the deposited to primary energy relationship was parametrised only for protons because this study considers the extensive air showers only from protons. The parametrised energy relationship is shown in figure 6.2b and is given by the following linear relation for protons entering the IceCube detector at three given zenith angles (black lines) in the Gaisser plot:

$$y = mx + c \tag{6.1}$$

For each black line the slope was calculated by the following relation:

$$m = \frac{y_2 - y_1}{x_2 - x_1} \tag{6.2}$$

Knowing the slope of the line (m) and the point of interception (c), the primary energy can be calculated, for any given deposited energy, for the three given zenith angles in the Gaisser energy plot using equation 6.1. Figure 6.2c shows the extrapolation of the energy of a proton (primary particle) using this linear relationship, for an in-ice deposited energy of 174 TeV, for a range of zenith angles. For example, for an in-ice event with deposited energy 174 TeV and cos of zenith 0.20, the extrapolated energy of the primary particle will be roughly 5×10^7 TeV.

Figure 6.2d shows the calculated energies of primary protons using the following quadratic fit for the relation shown in figure 6.2c:

$$E_p = a\text{zenith}^2 + b\text{zenith} + c \tag{6.3}$$

The constants a, b, and c are defined in appendix B. The code for extrapolation of energies of primary protons is shown in appendix B.

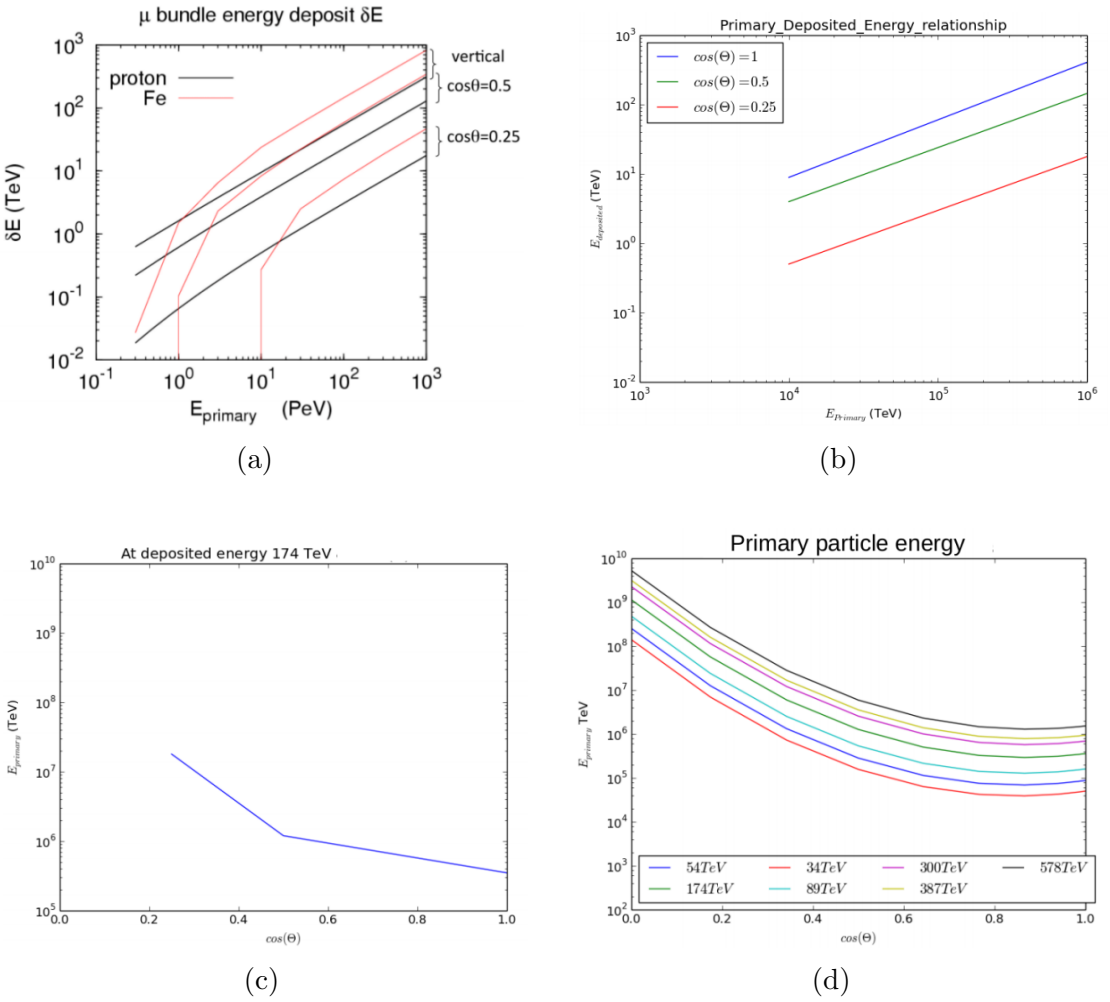

Figure 6.2: Extrapolation of energies of CR primary protons using the Gaisser energy relationship plot. (a) The Gaisser deposited and primary energy relationship plot. (b) Reproduced deposited and primary energy relationship for protons only. (c) Extrapolation of the energy of a primary proton using a linear relationship. (d) Extrapolation of the energies of primary protons using a quadratic fit.

6.2.2 Checking IceTop hits

Output from the air shower simulation code was used to produce figures 6.3 and 6.4 which show the expected number of muons and electrons IceTop hits along with one or more and two or more muon hit probability for the partially contained events. Here the red and blue dots represent the electrons and muons hits respectively. The yellow star represents the shower core intersection point on ice-surface.

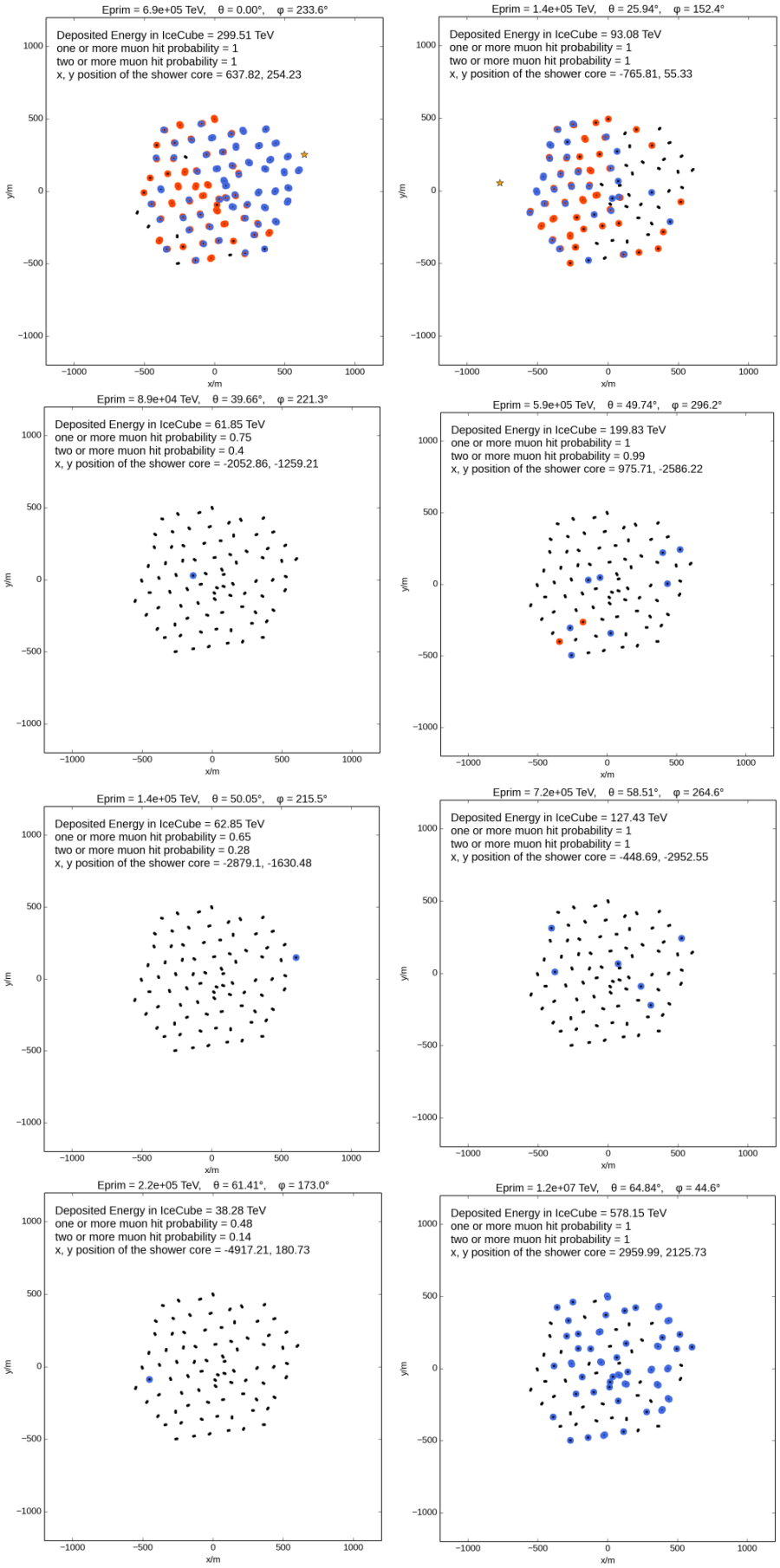

Figure 6.3: Expected number of IceTop hits for partially contained events.

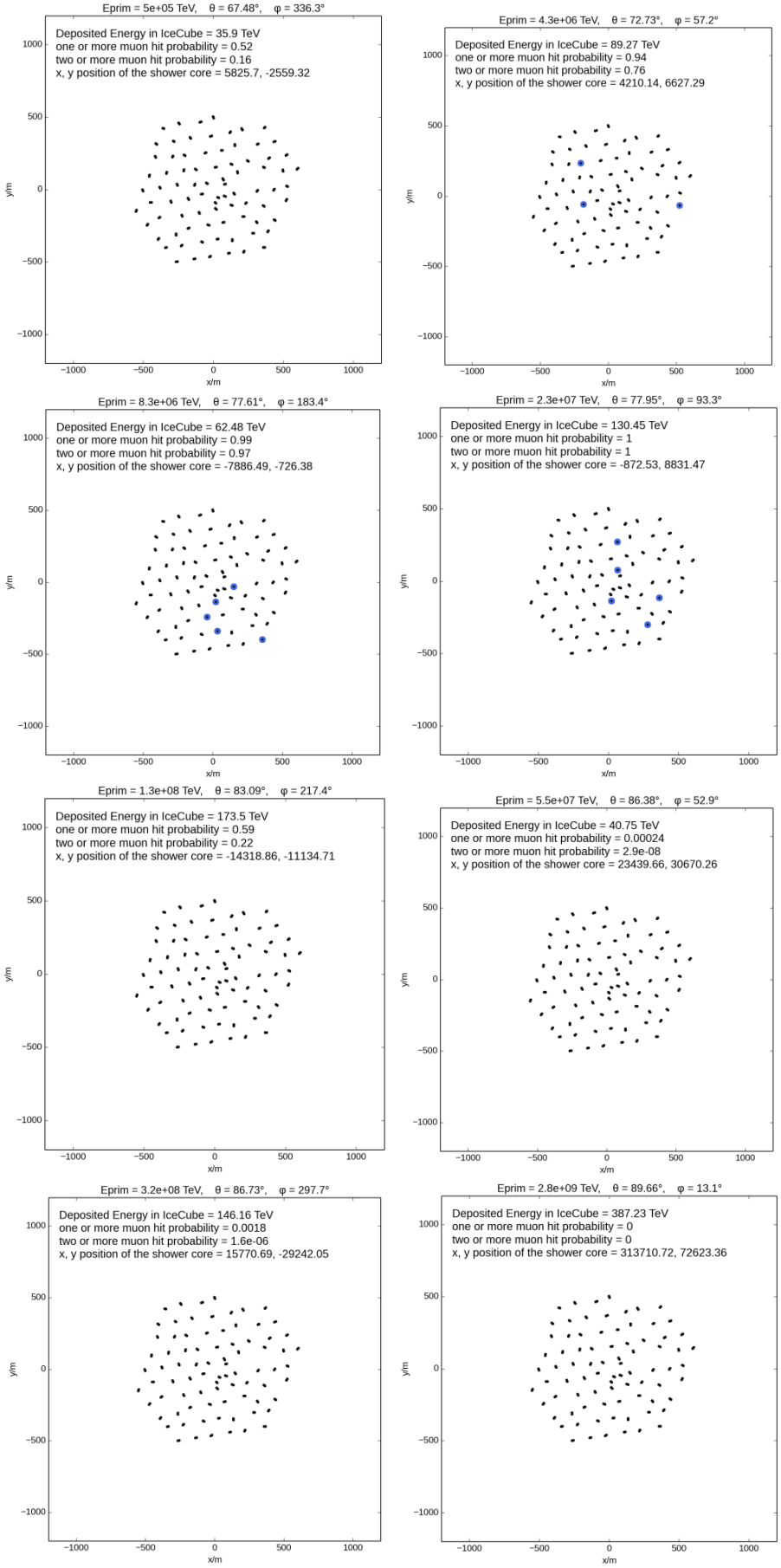

Figure 6.4: Expected number of IceTop hits for partially contained events.

6.2.3 IceTop hit probability

IceTop hit probability figures similar to those produced in figure 5.3 were produced with the partially contained event sample variables overlaid. Figure 6.5 show these plots where the probability shown is the probability of one or more muon hits. Here the stars represent the partially contained final events with their radial distance, deposited energy and their calculated primary energies. Here the radial distance is the distance of the shower core from IceTop centre. It can be seen that for some of the events, if they are indeed background events then there should be correlated hits in IceTop.

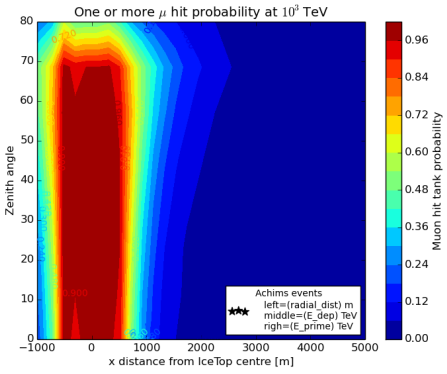

(a) 10^3

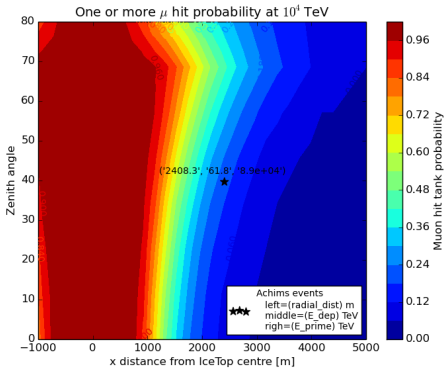

(b) 10^4

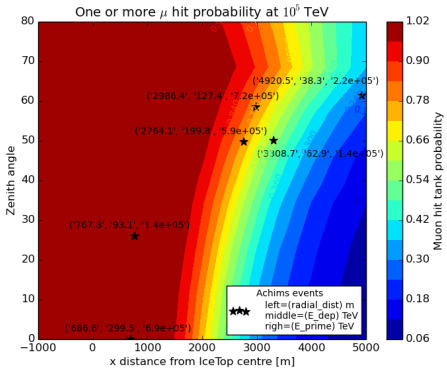

(c) 10^5

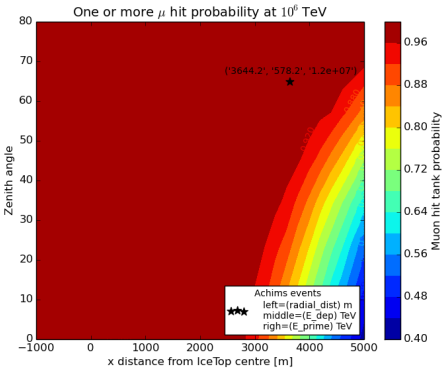

(d) 10^6

Figure 6.5: Probability of seeing at least one or more muon hits for partially contained cascade events at fixed energies.

6.2.4 Check on IceTop correlated hits

The information in the previous subsections motivated a search in the IceTop event files associated with the partially contained events. This information was not available for all of the events and for the events which the information was available, it was not possible to determine which tanks had been hit. For this reason timing information was only used for the centre of the array. For future studies it will be more useful to look at the hits in each tank with the timing expected on that tank rather than with respect to the centre of the array. The expected timing of associated hits at the IceTop array centre was calculated for each event using the procedure explained in section 5.2.1. The angular direction information has a larger uncertainty compared to track events. In section 5.2.2 it was found that the associated hits arrived in a time window of -500ns to 800ns around the expected time. However there is also a time uncertainty associated with the direction uncertainty. In figure 6.6 the calculated time for the shower front at the centre of the array for the zenith angle reconstructed for the partially contained events, and also for a zenith angle which was $\pm 10^{\circ}$ of this time is shown along with the observed IceTop hits. The plot is for the four events which had the closest IceTop hits to the calculated times. For the other events there was either no IceTop hits available or the IceTop hits were further from the calculated times. The black solid line in figure 6.6 shows the time of the event recorded in the IceCube InIce detector, the red dashed line is the expected shower core time at the IceTop surface, the green dashed line is the shower front time at the centre of the IceTop array while the purple and blue lines indicate the shower front time for a zenith angle which is $\pm 10^{\circ}$ respectively, from that calculated for the event. The black dots indicate the timing of any hits in IceTop around the InIce event time, with the vertical axis showing the charge of the IceTop hits. The zenith angle uncertainty of 10° results in a timing uncertainty of around 1000 ns, but in fact the zenith angle uncertainty is likely to be larger than this as this is the lower limit in the uncertainty which is quoted for the angular uncertainty for contained cascade events, and partially contained cascade events are likely to be harder to reconstruct.

It should be made clear that most of the black dot hits appearing in figure 6.6 will not be related to the InIce event recorded. The average spacing of the black dot hits gives an indication of the ambient rate of hits on IceTop. It is clear that if a large time window is used to classify IceTop hits as being correlated with an InIce event then the chance of removing true neutrino signal events will also become large. Our envisaged criteria was that if there were two IceTop hits within the $\pm 1000ns$ associated with the 10° uncertainty. In this preliminary investigation,

this condition would mean the event shown in 6.6 (d) would be classified as background. Further investigation is needed to find the optimal time window which allows for the uncertainty in zenith angle and is optimised in terms of the overall IceTop rate. This would be best on a per tank basis rather than using a global time for the whole array as was necessary in this study due to the information that was available.

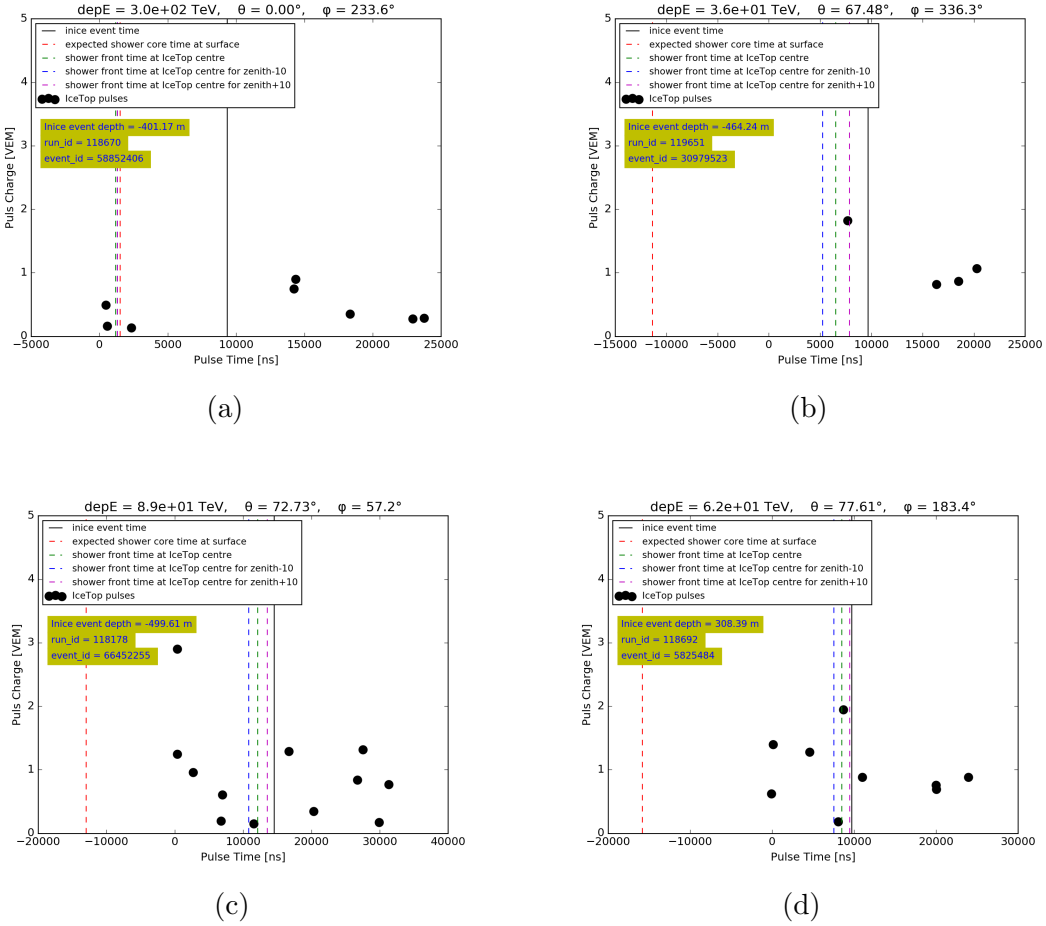

Figure 6.6: Black dots represent the IceTop hits.The black solid line indicates the inice event time, the red dashed line is the expected shower core time at the IceTop surface, the green dashed line is the shower front time at IceTop centre while the purple and blue lines indicate the shower front time for a zenith angle which is $\pm 10^{\circ}$ respectively, from that calculated for the event.

7 Discussion and Outlook

The work presented in this thesis is focused on the use of the IceTop array to identify background hits particularly for cascade events. There is other work ongoing in the IceCube collaboration to use IceTop as a veto focused on track-like events [45].

A simulation code was presented which allows a quick assessment of the likelihood for cosmic ray events to produce hits in IceTop. The dependent variables for the cosmic ray event are the energy and zenith angle of the primary cosmic ray particle and the surface intercept. probability of the cascade events as being background in nature. This code was benchmarked using a sample of high-energy IceCube events with good angular reconstruction. It was found that the simulation code performed well although there was a tendency to underestimate the hits in IceCube. The cause of this underestimation is unknown as it was expected that the opposite would be the case due to snow coverage of the IceTop tanks. It is possibly due to an underestimation of the primary energy of the cosmic ray particle. The study uses the IceTop air shower array to find the probability of cascade events as being background.

The simulation code was used to investigate the range in energy and zenith angle of the primary cosmic ray particle and the surface intercept over which the IceTop veto is likely to be useful and also to investigate the time bracket in which the hits arrive at IceTop compared to the time predicted for the shower front to intercept IceTop tanks. A time window of -500 ns to 800 ns was found to be appropriate.

Finally a preliminary study was made of the IceTop hits associated with a partially contained cascade event sample produced but Achim Stoessl. It was found that

one of the events had two hits in the time range within the $\pm 1000ns$ associated with the 10° uncertainty in the direction reconstruction of the cascade events.

The next steps for the use of IceTop as a veto will be to optimise the time window taking into account the background rate of hits on the IceTop array. It will be also important to consider the analysis criteria which are used in the cascade analyses as it is likely to be the case that many of the events which IceTop can remove are already removed by the cascade analysis criteria for rejecting events as background. Investigation should be made into whether any of the cascade analysis criteria can be relaxed allowing more signal to be retained, with the extra background being removed instead by the IceTop veto.

Appendices

A

Parametrisation based simulation Code for EAS

```
##########################################################################
# TITLE: Extensive Air Shower Simulation
# DESCRIPTION: Cosmic ray particles interact with the upper
    atmosphere and lead to the production of Extensive Air Showers.
    These showers consist of daughter particles that can be detected
    at the Earth's surface using large arrays of detectors. This code
    describes a method of simulating these Extensive Air Showers by
    estimating the lateral and longitudinal developments of the shower
    , and using Poisson statistics as the triggering mechanism.

# AUTHOR: Sebastian Euler, Benjamin Roberts, Kiran Munawar
# DATE: 16 March 2016

##########################################################################

#Imports the various modules and packages to use including the
    mathematical 'pylab' and 'optsparse' for the input parameters.
from __future__ import division
import pylab
from pylab import *
from optparse import OptionParser, OptionGroup
import math
import numpy as np
from numpy import *
#import primary_energy_using_quadratic_relation.py
#from primary_energy_using_quadratic_relation import GetEP
#import n_or_more as nom

muex2prim = np.genfromtxt("/home/kmu38/Desktop/IceVeto_project/
    looping_over_energies_and_zenith_angles_lists/
    Different_variable_relationships/xdist_energy_coszen/Analysis/
```

```
    analysis/muex2prim.txt", names=True)

def count_nonzero(arr):
    return size(arr[arr!=0])


matplotlib.rcParams['font.family'] = 'Liberation Sans'

######################################################################
# The following lines of code uses the Option Parser to create the
    various input parameters and their respective commands. Their
    default settings are also defined as well as help messages
    describing the parameters.
######################################################################

parser = OptionParser(usage='%prog [OPTIONS]', description=__doc__)
parser.add_option('-d', '--detector', choices=('grid', 'IceVeto', '
    IceTop'), default='grid', dest='DET',
                  help='Detector type [default: %default]')
parser.add_option('-a', '--stationarea', type=float, default=1., dest
    ='AREA',
                  help='Sensitive area of the new detector stations
                      in m^2 [default: %default]')
parser.add_option('-z', '--stationthickness', type=float, default=1.,
     dest='THICKNESS',
                  help='Thickness of the new detector stations in m [
                      default: %default]')
parser.add_option('-s', '--showers', type=int, default=1, dest='
    SHOWERS',
                  help='Number of showers [default: %default]')
parser.add_option('-E', '--energy', type=float, default=1e6, dest='E'
    ,
                  help='Shower primary energy in TeV [default: %
                      default]')
parser.add_option('--nuc', type=int, default=1, dest='NUCLEUS',
                  help='Atomic Size of Primary Particle [default: %
                      default]')
parser.add_option('-x', type=float, default=0.0, dest='X',
                  help='Minimum radius (cosine) [default: %default]')
parser.add_option('-y', type=float, default=0.0, dest='Y',
                  help='Maximum radius [default: %default]')
parser.add_option('--zen', type=float, default=0.5, dest='ZEN',
                  help='Zenith angle (cosine) [default: %default]')
parser.add_option('--azi', type=float, default=0.0, dest='AZI',
                  help='Azimuthal angle [default: %default]')
parser.add_option('--threshold', type=int, default=1, dest='THR',
                  help='Trigger threshold for all triggers [default:
                      %default]')
```

```
parser.add_option('--auto', action='store_true', default=False, dest=
    'AUTO',
                  help='Automatically calculate min/max radius and
                      azimuth angle such that showers point towards
                      IceCube [default: %default]')

groupG = OptionGroup(parser, 'Options for the grid detector',
                      'The following options are used for the grid
                          detector only. NOTE: Detectors with a spacing
                           < 100m will be named "SuperVeto"!')
groupG.add_option('--gridsize', type=int, default=5000, dest='SIZE',
                  help='Extension of the grid (half side length) [
                      default: %default]')
groupG.add_option('-n', '--stations', type=int, default=50, dest='
    STATIONS',
                  help='Number of stations along one side of the grid
                       [default: %default]')
parser.add_option_group(groupG)

groupV = OptionGroup(parser, 'Options for the IceVeto & IceTop
    detectors',
                      'The following options are used for the IceVeto
                          & IceTop detectors only')
groupV.add_option('--coordFile', default='/home/kmu38/Desktop/
    IceVeto_project/looping_over_energies_and_zenith_angles_lists/
    Different_variable_relationships/xdist_energy_coszen/Analysis/
    analysis/coords_IceVeto.txt', dest='COORDS',
                  help='Location of the input file containing the
                      IceVeto & IceTop coordinates. [default: %default
                      ]')
groupV.add_option('--noIceTop', action='store_true', default=False,
    dest='NOIT',
                  help='Exclude the IceTop tanks from the IceVeto
                      geometry [default: %default]')
groupV.add_option('--plotHEX', action='store_true', default=False,
    dest='HEX',
                  help='Plot the HEX outline (240m spacing, 120
                      strings) [default: %default]')
parser.add_option_group(groupV)

groupT = OptionGroup(parser, 'Options for saving the trigger
    efficiency in a text file',
                      'The following options are used for saving the
                          calculated trigger efficiency to a txt file')
groupT.add_option('--txt', action='store_true', default=False, dest='
    TXT',
                  help='Only return the trigger efficiency, no
                      plotting or anything fancy [default: %default]')
```

```
groupT.add_option('--outputDir', default='/home/kmu38/Desktop/
    IceVeto_project/looping_over_energies_and_zenith_angles_lists/
    Different_variable_relationships/xdist_energy_coszen/Analysis/
    analysis/TXT/', dest='OUTDIR',
                      help='The output directory for the calculated
                          trigger efficiency files [default: %default].
                          NOTE: Typically, a few thousand output files
                          will be produced!')
groupT.add_option('--summary', default='summary.txt', dest='
    SUMMARYFILE',
                      help='The output file for the calculated trigger
                          efficiency files [default: %default].')
parser.add_option_group(groupT)


opts, args = parser.parse_args()
if opts.DET=='IceTop' and opts.NOIT:
    parser.error('You selected the detector type "IceTop", but
        removed it with the "--noIceTop" option. Now there is no
        detector left!')
if opts.TXT and opts.SHOWERS==1:
    parser.error('I cannot calculate a trigger efficiency from 1
        shower only. Use the "--showers" (or "-s") option to increase
        the number of showers.')

# The following sets of coordinates follow the outline of the HEX
    array (Sunflower 240m) and are used when the '--plotHEX' command
    is used.
HEXx = [704, 752, 742, 681, 574, 427, 243, 29, -328, -646, -884,
    -1133, -1353, -1501, -1566, -1697, -1638, -1689, -1508, -1266,
    -1183, -858, -666, -486, -323, -180, 4, -9, 361, 576, 704]
HEXy = [500, 703, 907, 1106, 1293, 1460, 1603, 1715, 1625, 1462,
    1444, 1178, 1075, 734, 380, 178, -184, -423, -751, -1020, -1248,
    -1424, -1346, -1229, -1065, -836, -733, -482, -423, 171, 500]

##################################################################
# Detector Array Shape

# Initialses the spacing quantity
if opts.DET!='grid':
    spacing=''

# Calculates or reads the coordinates of each detector in the array
    as an (x,y) pair
if opts.DET=='grid':
    spacing = int(2*opts.SIZE/opts.STATIONS)
    if spacing < 100:
        opts.DET = 'SuperVeto'
    print '-------------------------------'
```

```
    print 'Using {0} detector'.format(opts.DET)
    print 'size:', 2*opts.SIZE
    print 'stations:', opts.STATIONS**2
    print 'spacing:', spacing
    print '-------------------------------'
    x = linspace(-opts.SIZE, opts.SIZE, opts.STATIONS+1)
    y = linspace(-opts.SIZE, opts.SIZE, opts.STATIONS+1)
    x,y = meshgrid(x,y)
    area = ones(x.shape) * opts.AREA
    thickness = ones(x.shape) * opts.THICKNESS

elif opts.DET=='IceVeto' or opts.DET=='IceTop':
    print '---------------------------------------'
    print 'Using {0} detector'.format(opts.DET)
    print '---------------------------------------'
    n = []
    x = []
    y = []
    with open(opts.COORDS) as f:
        for line in f:
            l = line.split(',')
            n.append(int(l[0]))
            x.append(float(l[1]))
            y.append(float(l[2]))
    if opts.NOIT:
        opts.DET = 'IceVeto_noIT'
        n = n[162:]
        x = x[162:]
        y = y[162:]
    if opts.DET=='IceTop':
        opts.SIZE = 1000
        n = n[:162]
        x = x[:162]
        y = y[:162]
    x = array(x)
    y = array(y)
    area = array([2.6 if i<162 else opts.AREA for i in n])
    thickness = array([1.0 if i<162 else opts.THICKNESS for i in n])


#############################################################

from icecube import icetray, dataclasses, dataio
import glob


fileList = glob.glob("/home/kmu38/Desktop/IceVeto_project/
    looping_over_energies_and_zenith_angles_lists/
    Different_variable_relationships/xdist_energy_coszen/Analysis/
```

```
    analysis/burn_ehe.i3.bz2")
particleCounter = 0

print opts.OUTDIR

for f in fileList:
    i3f = dataio.I3File(f)
    for frame in i3f:
  #print "Frame No: ", particleCounter
        #if particleCounter == 10: break

        if frame.Stop==icetray.I3Frame.Physics:
            h = frame["I3EventHeader"]
            eventid = h.event_id
            subeventid = h.sub_event_id
            #print 'event_id:', eventid
        #if not frame.Has('SPEFit12EHE_refit_MPE'): continue
            recoParticle = frame['MuEx_sp3_SPEFit12EHE_refit_MPE'] #
                <== MIGHT HAVE TO CHANGE THIS, DEPENDING ON THE NAME
                OF THE RECONSTRUCTED I3PARTICLE YOU WANT TO USE
            particleCounter+=1

            # take position and direction of the event you want to re
                -simulate

            inIcePos = array([recoParticle.pos.x, recoParticle.pos.y,
                 recoParticle.pos.z])
            inIceDir = array([recoParticle.dir.x, recoParticle.dir.y,
                 recoParticle.dir.z])
            Zen = recoParticle.dir.zenith
      if Zen < 0:
    print "Zenith angle", Zen, "is negative!"
    continue
            if Zen <= 0.1:
                zen = 0.1
            zenith = Zen
            if not 30*(np.pi/180.) <= zenith <= 40*(np.pi/180):
          continue
            azimuth = recoParticle.dir.azimuth

            ##########################################################
            # By dividing Ed by 1000 we convert deposited energy from
                 GeV to TeV.
            ##########################################################

            #depE = (recoParticle.energy)/1000
            depE = recoParticle.energy
            log_depE = np.log10(depE)
            print 'depE:', depE
```

```
        Muex = np.around(depE, decimals=2)

        # calculate position at the surface

        s = (1950 - inIcePos[2])/inIceDir[2]
        surfacePos = inIcePos + s*inIceDir

        sx = (surfacePos[0])*ones(opts.SHOWERS)
        sy = (surfacePos[1])*ones(opts.SHOWERS)
        coszen = np.cos(zenith*ones(opts.SHOWERS))
        azi = azimuth*ones(opts.SHOWERS)
plow = pmed = phigh = -1
        isval = False
for line in muex2prim:
    if line['xmin'] <= np.log10(Muex) <= line['xmax']:
  plow = line['plow']
  pmed = line['pmed']
  phigh = line['phigh']
  isval = True
if not isval: continue
Final_Energy_primary = plow/1000. #GeV -> TeV

        ######################################################

        # Calculate the lateral and longitudinal distributions
            for each detector and simulates the triggering of each
             detector

        # Initialises the number of triggered detectors for each
            method
        poissontrig_e = 0
        poissontrig_mu = 0

#print opts.OUTDIR+'{0}_{1:.2f}_{2}.txt'.format(particleCounter
    , rad2deg(zenith), np.log10(Muex))
        with open(opts.OUTDIR+'{0}_{1:.2f}_{2:.2f}.txt'.format(
            particleCounter, rad2deg(zenith), np.log10(Muex)),'w')
             as summary:
            # Calculates the distance to all tanks from each of
                the showers intersection with the detector plane
            for shower in zip(sx, sy, coszen, azi):

                dx = (x - shower[0]).flatten()
                dy = (y - shower[1]).flatten()
                dz = zeros_like(dx)

                # Calculates the unit direction vector of the
                    shower axis
```

```
r = array([sin(arccos(shower[2]))*cos(shower[3]),
     sin(arccos(shower[2]))*sin(shower[3]), shower
    [2]]).flatten()

# Calculates the lateral distances for each
    detector and determines if the shower has
    developed past its intersection with the
    detector plane
D = []
sign = []
for p in zip(dx, dy, dz):
    D.append(linalg.norm(cross(p, r)))
    if p[1] + p[0]/tan(shower[3]) > 0:
        if (shower[3] >=0) and (shower[3]<pi):
            sign.append(1)
        else:
            sign.append(-1)
    elif p[1] + p[0]/tan(shower[3]) < 0:
        if (shower[3] >=0) and (shower[3]<pi):
            sign.append(-1)
        else:
            sign.append(1)
    else:
        sign.append(0)
d = reshape(D, x.shape)
deltx = reshape(dx, x.shape)
delty = reshape(dy, x.shape)
sign = reshape(sign, x.shape)

# Approximates the slanted Overburden and
    calculates the longitudinal distribution
A = opts.NUCLEUS
X_0_e = 100
X_0_mu = -200
lambd_e = 70
lambd_mu = 1109
N_max_e = 27.6798 * Final_Energy_primary**(17/15)
N_max_mu = (A**(1-0.75))*(0.95 * 10**5)*(N_max_e
    /(10**6))**0.75
X_max = 212 + 25*log((Final_Energy_primary/A)
    /(10**-3))

l = sqrt(deltx**2 + delty**2 - d**2)
height = l*shower[2]
h = (sign*height+2835)/1000
interm = (h <= 3.96)
X_v= (146.66 + 932.8 * exp(-h/5.208))*interm +
    (-110.33 + 1119.8 * exp(-h/8.255))*(1-interm)
X_s = X_v/shower[2]
```

```
N_e = N_max_e*(((X_s-X_0_e)/(X_max-X_0_e))**((
    X_max-X_0_e)/lambd_e))*exp((X_max-X_s)/lambd_e
    )
N_mu = N_max_mu*(((X_s-X_0_mu-X_max)/(-X_0_mu))
    **((-X_0_mu)/lambd_mu))*exp((X_max-X_s)/
    lambd_mu)

# Defines the Moliere radius value at the South
    Pole
r_M = 105

# Calculates the Lateral Distribution  at each
    detector (in particles/m^2)
rho_e = 0.4 * N_e / r_M**2 * (r_M/d)**0.75 * (r_M
    /(d+r_M))**3.25
# Use old recipe to get number of electrons for
    the muon ldf to circumvent suppression as for
    the electromagnetic part
#N_emu = (opts.E/1.3e-4)**(1/1.25)
#rho_mu = 18 * (N_emu/1e6)**0.75 * d**-0.75 * (1
    + d/320)**-2.5
rho_mu = (1.89*10**-4) * N_mu * d**-0.75 * (1 + d
    /320)**-2.5

# Calculates the effective area of the detector
    stations, depending on the shower zenith angle
# Assumes a square detector, with side length
    sqrt(area)
width = sqrt(area)
baseline = sqrt(thickness**2 + width**2)
epsilon = arcsin(thickness/baseline)
beta = pi/2 - arccos(shower[2]) + epsilon
alpha = pi/2 - beta
area_eff = baseline * cos(alpha) * width

# Simulates triggering by Poisson statistics
# Calculates the Poisson probability to achieve
    at least one detection at a detector
p_e = 1 - exp(-area_eff*rho_e)
p_mu = 1 - exp(-area_eff*rho_mu)
p_mu_e = 1 - ((1-p_mu)*(1-p_e))
#p_one_or_more_hits_onicetop = nom.one_or_more(
    p_mu_e)
#p_two_or_more_hits_onicetop = nom.two_or_more(
    p_mu_e)
#p_mu_one_or_more_hits_onicetop = nom.one_or_more
    (p_mu)
```

```
#p_mu_two_or_more_hits_onicetop = nom.two_or_more
    (p_mu)

# Triggers individual tanks with the previously
    obtained Poisson statistic

rand_e = random_sample(p_e.shape)
pois_e = rand_e<p_e
rand_mu = random_sample(p_mu.shape)
pois_mu = rand_mu<p_mu
if sum(pois_e) >= opts.THR:
    poissontrig_e += 1

if sum(pois_mu) >= opts.THR:
    poissontrig_mu += 1

# Get the indices of the electron and muon hit
    tanks, count only once if a tank is hit by
    both electron and muon.

hit_e = []
mask2 = pois_e == True
for F in zip(x[mask2], y[mask2]):
    hit_e.append(F)


hit_mu = []
mask3 = pois_mu == True
for M in zip(x[mask3], y[mask3]):
    hit_mu.append(M)


# Get the indices of the unhit tanks  if mask.any
    (False):
unhit_e = []
mask1 = pois_e == False
for A in zip(x[mask1], y[mask1]):
    unhit_e.append(A)
    #print A

unhit_mu = []
mask = pois_mu == False
# loop over them
for K in zip(x[mask], y[mask]):
    unhit_mu.append(K)
    #print K

Nhit = len(list(set(hit_e + hit_mu)))
Nunhit = len(set(unhit_e) & set(unhit_mu))
```

```
summary.write('{0} {1} {2} {3} {4} {5}\n'.format(
    eventid, subeventid, sum(area_eff*rho_mu), len
    (hit_mu), sum(area_eff*rho_e), len(hit_e) ))

# Prepares the Lateral Distribution Functions for
    plotting
if opts.SHOWERS==-1:
    cx = cy = linspace(-6000, 6000, 300)
    cx,cy = meshgrid(cx,cy)
    dx = (cx - shower[0]).flatten()
    dy = (cy - shower[1]).flatten()
    dz = zeros_like(dx)
    r = array([sin(arccos(shower[2]))*cos(shower
        [3]), sin(arccos(shower[2]))*sin(shower
        [3]), shower[2]]).flatten()
    D = []
    sign = []
    for p in zip(dx, dy, dz):
        D.append(linalg.norm(cross(p, r)))
        if p[1] + p[0]/tan(shower[3]) > 0:
            if (shower[3] >=0) and (shower[3]<pi)
                :
                sign.append(1)
            else:
                sign.append(-1)
        elif p[1] + p[0]/tan(shower[3]) < 0:
            if (shower[3] >=0) and (shower[3]<pi)
                :
                sign.append(-1)
            else:
                sign.append(1)
        else:
            sign.append(0)
    d = reshape(D, cx.shape)
    deltx = reshape(dx, cx.shape)
    delty = reshape(dy, cx.shape)
    sign = reshape(sign, cx.shape)
    A = opts.NUCLEUS
    X_0_e = 100
    X_0_mu = -200
    lambd_e = 70
    lambd_e = 1109
    N_max_e = 27.6798 * Final_Energy_primary
        **(17/15)
    N_max_mu = (A**(1-0.75))*(0.95 * 10**5)*(
        N_max_e/(10**6))**0.75
    X_max = 212 + 25*log((Final_Energy_primary/A)
        /(10**-3))
    l = sqrt(deltx**2 + delty**2 - d**2)
```

```
                        height = l*shower[2]
                        h = (sign*height + 2835)/1000
                        interm = (h <= 3.96)
                        X_v= (146.66 + 932.8 * exp(-h/5.208))*interm
                            + (-110.33 + 1119.8 * exp(-h/8.255))*(1-
                            interm)
                        X_s = X_v/shower[2]
                        N_e = N_max_e*(((X_s-X_0_e)/(X_max-X_0_e))
                            **((X_max-X_0_e)/lambd_e))*exp((X_max-X_s)
                            /lambd_e)
                        N_mu = N_max_mu*(((X_s-X_0_mu-X_max)/(-X_0_mu
                            ))**((-X_0_mu)/lambd_mu))*exp((X_max-X_s)/
                            lambd_mu)
                        rho_e = 0.4 * N_e / r_M**2 * (r_M/d)**0.75 *
                            (r_M/(d+r_M))**3.25
                        # Use old recipe to get number of electrons
                            for the muon ldf to circumvent suppression
                             as for the electromagnetic part
                        #N_emu = (opts.E/1.3e-4)**(1/1.25)
                        #rho_mu = 18 * (N_emu/1e6)**0.75 * d**-0.75 *
                             (1 + d/320)**-2.5
                        rho_mu = (1.89*10**-4) * N_mu * d**-0.75 * (1
                             + d/320)**-2.5

                        Final_Energy_Primary = '%.2g' %
                            Final_Energy_primary
                        #P_mu_one_or_more_hits_onicetop = '%.2g' %
                            p_mu_one_or_more_hits_onicetop
                        #P_mu_two_or_more_hits_onicetop = '%.2g' %
                            p_mu_two_or_more_hits_onicetop
                        x_position_of_shower_core = np.around(
                            surfacePos[0], decimals=2)
                        y_position_of_shower_core = np.around(
                            surfacePos[1], decimals=2)
                        #x_position_of_shower_core = '%.2g' %
                            surfacePos[0]
                        #y_position_of_shower_core = '%.2g' %
                            surfacePos[1]
######################################################################
                        #Creates the relevant plots

                        if not opts.TXT:

                            if opts.SHOWERS==1:

                                #Plots the detector grid and the
                                    triggered detectors
                                fig1 = figure(figsize=(8,8))
```

```
title(u'Eprim = {0} TeV,     \u03b8 =
    {1:.2f}\u00b0,     \u03c6 = {2:.1f
    }\u00b0'.format(
    Final_Energy_Primary, rad2deg(
    zenith), rad2deg(azimuth)))
#title('Eprim = %.2g TeV, u\u03b8 =
    {1:.2f}\u00b0' % (
    Final_Energy_primary, rad2deg(
    zenith))
plot(x, y, marker='.', linestyle='
    None', label='station', color='k')
plot(x[pois_e], y[pois_e], marker='o'
    , linestyle='None', label='station
    ', mec='orangered', mfc='None',
    mew=3)
plot(x[pois_mu], y[pois_mu], marker='
    o', linestyle='None', label='
    station', mec='royalblue', mfc='
    None', mew=3)
plot(sx, sy, marker='*', linestyle='
    None', label='shower', color='
    orange', markersize=10)
xlabel('x/m')
ylabel('y/m')
xlim(-1.2*opts.SIZE,1.2*opts.SIZE)
ylim(-1.2*opts.SIZE,1.2*opts.SIZE)
pylab.gcf().text(0.15, 0.85, '
    Deposited Energy in IceCube = %s
    TeV' % DepE, fontsize=15)
pylab.gcf().text(0.15, 0.82, 'one or
    more muon hit probability = %s' %
    P_mu_one_or_more_hits_onicetop,
    fontsize=15)
pylab.gcf().text(0.15, 0.79, 'two or
    more muon hit probability = %s' %
    P_mu_two_or_more_hits_onicetop,
    fontsize=15)
pylab.gcf().text(0.15, 0.76, 'x, y
    position of the shower core = %s,
    %s' % (x_position_of_shower_core,
    y_position_of_shower_core),
    fontsize=15)
figname = ('{0:.2f}_{1:.2f}
    _in_degrees.png'.format(rad2deg(
    zenith), rad2deg(azimuth)))
savefig(figname, dpi=192)
print 'wrote', figname
```

```
                else:
                    print 'Total no of hit tanks:'  ,len(
                        list(set(hit_e + hit_mu)))
                    print 'Total no of unhit tanks:',len(
                        set(unhit_e) & set(unhit_mu))


            else:
                f = open(opts.OUTDIR+'/{0}{1}_{2}_{3}.txt
                    '.format(opts.DET, spacing, opts.E,
                    opts.ZENMIN), 'w')
                f.write('{0}\t{1}\t{2}\t{3}\t{4}\n'.
                    format(opts.E, opts.ZENMIN, opts.
                    ZENMAX,
                                        poissontrig_e/opts.
                                            SHOWERS,
                                            poissontrig_mu/opts
                                            .SHOWERS))
                f.close()
```

B

Extrapolation of the energy of the primary particle

```
#####################################################
# Title: Calculating Primary energies corresponding to given
    deposited energies.
# Description: This code calculates the primary energies of particle
    showers of IceCube events with given deposited energies using Tom
    Gaisser's Deposited_Primary energy relationship.
# Author: Kiran Munawar
# Date: 25 May, 2016
#####################################################

import matplotlib as mpl
mpl.use('Agg')
import numpy
from numpy import *
import matplotlib.pyplot as plt
import math
from math import *

#####################################################
# Put in the deposited energies of Achim's events
#####################################################

E_d = [54, 174, 200, 62, 53, 41, 93, 146, 34, 38, 89, 127, 300, 387,
    62, 578, 130, 116, 63]
log_E_d = numpy.log10(E_d)

#####################################################
# The following functions calculate the slopes and points of
    intercept of each line in Tom Gaisser's deposited versus primary
    energy plot
#####################################################
```

```
#####################################################
# for line 1 with cos(theta) = 1
#####################################################

def E1(E_d_1):
    m = 0.83
    c = -2.37
    m1 = 1/m
    c1 = -c/m
    E_p = m1*E_d_1 + c1
    return E_p

#####################################################
# for line 2 with cos(theta) = 0.5
#####################################################

def E2(E_d_2):
    m = 0.78
    c = -2.52
    m1 = 1/m
    c1 = -c/m
    E_p = m1*E_d_2 + c1
    return E_p

def E3(E_d_3):
    m = 0.775
    c = -3.4
    m1 = 1/m
    c1 = -c/m
    E_p = m1*E_d_3 + c1
    return E_p

def EP(x):
    Final_ep = a*(x)**2 + b*(x) + c
    return 10**Final_ep

#####################################################
# put in the angles of each event
#####################################################

theta_rec = [111, 83, 50, 40, 247, 86, 26, 87, 145, 61, 73, 59, 0,
   90, 78, 65, 78, 67, 100, 50]
cos_theta_rec = [numpy.cos(x*numpy.pi/180.0) for x in theta_rec]

with open('Primary_energies_from_quadratic_fit.txt', 'w') as summary:
    for Ed, cos_rec in zip(log_E_d, cos_theta_rec):
        y_1 = E1(Ed)
        y_2 = E2(Ed)
```

```
y_3 = E3(Ed)

x_1 = 1.0
x_2 = 0.5
x_3 = 0.25

a = y_1/((x_1-x_2)*(x_1-x_3)) + y_2/((x_2-x_1)*(x_2-x_3)) +
    y_3/((x_3-x_1)*(x_3-x_2))

b = (-y_1*(x_2+x_3)/((x_1-x_2)*(x_1-x_3))
     -y_2*(x_1+x_3)/((x_2-x_1)*(x_2-x_3))
     -y_3*(x_1+x_2)/((x_3-x_1)*(x_3-x_2)))

c = (y_1*x_2*x_3/((x_1-x_2)*(x_1-x_3))
     +y_2*x_1*x_3/((x_2-x_1)*(x_2-x_3))
     +y_3*x_1*x_2/((x_3-x_1)*(x_3-x_2)))

print 'Ed: ', 10**Ed
print 'a:', a
print 'b:', b
print 'c:', c
if cos_rec >= 0.0:
    Final_E_Prime = EP(cos_rec)
    summary.write('{0},{1},{2}\n'.format(Final_E_Prime,
        rad2deg(arccos(cos_rec)), 10**Ed))
```

Bibliography

[1] A. M. Hillas, *Cosmic Rays: Recent Progress and some Current Questions*, in *Conference on Cosmology, Galaxy Formation and Astro-Particle Physics on the Pathway to the SKA Oxford, England, April 10-12, 2006* (2006) [astro-ph/0607109].

[2] J. M. Santander, *Observation of Cosmic-Ray Anisotropy at TeV and PeV Energies in the Southern Sky*. PhD thesis, University of Wisconsin–Madison, 2013.

[3] h. Infrared: NASA/JPL-Caltech/Steward/O. Krause et al., 2005.

[4] J. K. Becker, *High-energy neutrinos in the context of multimessenger physics*, *Phys. Rept.* **458** (2008) 173–246, [arXiv:0710.1557].

[5] J. Matthews, *A Heitler model of extensive air showers*, *Astroparticle Physics* **22** (2005) 387–397.

[6] R. Abbasi, Y. Abdou, *et. al.*, *IceTop: The surface component of IceCube. The IceCube Collaboration*, *Nuclear Instruments and Methods in Physics Research A* **700** (2013) 188–220, [arXiv:1207.6326].

[7] **IceCube** Collaboration, M. G. Aartsen *et. al.*, *Observation of High-Energy Astrophysical Neutrinos in Three Years of IceCube Data*, *Phys. Rev. Lett.* **113** (2014) 101101, [arXiv:1405.5303].

[8] **IceCube** Collaboration, M. G. Aartsen *et. al.*, *IceCube-Gen2: A Vision for the Future of Neutrino Astronomy in Antarctica*, arXiv:1412.5106.

[9] S. Bilenky, *Neutrino. History of a unique particle*, *Eur.Phys.J.* **H38** (2013) 345–404, [arXiv:1210.3065].

[10] C. Cowan, F. Reines, F. Harrison, H. Kruse, and A. McGuire, *Detection of the free neutrino: A Confirmation*, *Science* **124** (1956) 103–104.

[11] T. K. Gaisser, *Cosmic Rays And Particle Physics*. Cambridge University Press, 1990.

[12] **Fermi-LAT** Collaboration, M. Ackermann *et. al.*, *Detection of the Characteristic Pion-Decay Signature in Supernova Remnants*, *Science* **339** (2013) 807, [arXiv:1302.3307].

[13] G. Kulikov and G. Khristiansen, *On the size spectrum of extensive air showers*, *SOVIET PHYSICS JETP-USSR* **8** (1959) 441–444.

[14] T. Stanev, *High Energy Cosmic Rays*. Springer Praxis Books. Springer Berlin Heidelberg, 2010.

[15] A. W. Strong, I. V. Moskalenko, and V. S. Ptuskin, *Cosmic-ray propagation and interactions in the galaxy*, *Annu. Rev. Nucl. Part. Sci.* **57** (2007) 285–327.

[16] K. Greisen, *End to the Cosmic-Ray Spectrum?*, *Physical Review Letters* **16** (1966) 748–750.

[17] K. Zatsepin, *Upper Limit of the Spectrum of Cosmic Rays*, *JETP Letters* **4** (1966) 78.

[18] **Pierre Auger** Collaboration, J. Abraham *et. al.*, *Observation of the suppression of the flux of cosmic rays above* $4 \times 10^{19} eV$, *Phys. Rev. Lett.* **101** (2008) 061101, [arXiv:0806.4302].

[19] A. M. Hillas, *The Origin of Ultrahigh-Energy Cosmic Rays*, *Ann. Rev. Astron. Astrophys.* **22** (1984) 425–444.

[20] E. Fermi, *On the Origin of the Cosmic Radiation*, *Physical Review* **75** (1949) 1169–1174.

[21] A. Meli, J. K. Becker, and J. J. Quenby, *Ultra high energy cosmic rays: subluminal and superluminal shocks*, *ArXiv e-prints* (2009) [arXiv:0905.4466].

[22] A. Hillas, *The origin of ultra-high-energy cosmic rays*, *Annual Review of Astronomy and Astrophysics* **22** (1984) 425–444.

[23] *High-energy neutrino astrophysics*, *Annual Review of Nuclear and Particle Science* **50** (2000) 679–749.

[24] R. W. Klebesadel, I. B. Strong, and R. A. Olson, *Observations of gamma-ray bursts of cosmic origin*, *The Astrophysical Journal* **182** (1973) L85.

[25] P. Meszaros and M. Rees, *Relativistic fireballs and their impact on external matter-models for cosmological gamma-ray bursts*, *The Astrophysical Journal* **405** (1993) 278–284.

[26] K.-H. Kampert, *Methods of determination of the energy and mass of primary cosmic ray particles at extensive air shower energies*, *Journal of Physics G: Nuclear and Particle Physics* **27** (2001) 1663.

[27] H. J. Bhabha and W. Heitler, *The passage of fast electrons and the theory of cosmic showers*, *Proceedings of the Royal Society of London A: Mathematical, Physical and Engineering Sciences* **159** (1937) 432–458, [http://rspa.royalsocietypublishing.org/content/159/898/432.full.pdf].

[28] W. Heitler, *The quantum theory of radiation*, .

[29] J. R. HÖRANDEL, *Cosmic rays from the knee to the second knee: 1014 to 1018ev*, *Modern Physics Letters A* **22** (2007) 1533–1551.

[30] B. Roberts, *University of canterbury 480 project*, .

[31] P. K. F. Grieder, *Cosmic rays at earth: Researcher's reference manual and data book. elsevier science limited*, .

[32] S. Euler, *Personal communication*, .

[33] T. K. Gaisser and A. M. Hillas, *in Proc. 15th Int. Cosmic Ray Conf., p. 358, Plovdiv, Bulgaria, 1977.*, (1977) 358.

[34] F. Schmidt, M. Ave, L. Cazon, and A. Chou, *A model-independent method of determining energy scale and muon number in cosmic ray surface detectors*, *Astroparticle Physics* **29** (2008) 355 – 365.

[35] K. Kamata and J. Nishimura, *The lateral and the angular structure functions of electron showers*, *Progress of Theoretical Physics Supplement* **6** (1958) 93.

[36] K. Greisen, *Cosmic ray showers*, *Annual Review of Nuclear Science* **10** (1960) 10–63.

[37] *Corsika*, . https://www.ikp.kit.edu/corsika/70.php.

[38] **IceCube** Collaboration, M. Aartsen *et. al.*, *Evidence for High-Energy Extraterrestrial Neutrinos at the IceCube Detector*, *Science* **342** (2013) 1242856, [arXiv:1311.5238].

[39] **ICECUBE** Collaboration, A. a. K. Haj Ismail, *Low Energy Air Showers with IceTop*, in *Proceedings, 33rd International Cosmic Ray Conference (ICRC2013): Rio de Janeiro, Brazil, July 2-9, 2013* 0674.

[40] **Pierre Auger** Collaboration, J. Abraham *et. al.*, *Properties and performance of the prototype instrument for the Pierre Auger Observatory*, *Nucl. Instrum. Meth.* **A523** (2004) 50–95.

[41] M. Ave, J. Knapp, J. Lloyd-Evans, M. Marchesini, and A. A. Watson, *The Energy spectrum of cosmic rays above 3 x 10**17-eV as measured with the Haverah Park array*, *Astropart. Phys.* **19** (2003) 47–60, [astro-ph/0112253].

[42] **The IceCube Collaboration** Collaboration, R. A. et al., *The IceCube Data Acquisition System: Signal Capture, Digitization, and Timestamping*, *Nucl.Instrum.Meth.A601:294-316,2009* (2009).

[43] R. Abbasi, Y. Abdou, *et. al.*, *Calibration and characterization of the IceCube photomultiplier tube*, *Nuclear Instruments and Methods in Physics Research A* **618** (2010) 139–152, [arXiv:1002.2442].

[44] **ICECUBE** Collaboration, J. Auffenberg, *IceTop as a veto in astrophysical neutrino searches for IceCube*, in *Proceedings, 33rd International Cosmic Ray Conference (ICRC2013): Rio de Janeiro, Brazil, July 2-9, 2013* 0373.

[45] D. Tossi, *Icetop as veto*, . https://wiki.icecube.wisc.edu/index.php/IceTop_Veto.

[46] **IceCube** Collaboration, D. Tosi and K. Jero, *IceTop as Veto for IceCube*, *PoS* **ICRC2015** (2016) 1086.

[47] **IceCube-Gen2** Collaboration, S. Euler, J. Gonzalez, and B. Roberts, *Simulation Studies for a Surface Veto Array to Identify Astrophysical Neutrinos at the South Pole*, *PoS* **ICRC2015** (2016) 1070.

[48] S. Euler, *Talk at icecube collaboration meeting, copenhagen, october, 2015*, .

[49] J. A. Stoessl, *A search for particle showers at the edge of icecube's instrumented volume*, . https://edoc.hu-berlin.de/handle/18452/18794.

ACKNOWLEDGEMENTS

I would first like to thank my thesis supervisor Dr. Jenni Adams. She was always willing to help me whenever I had a question about my research or writing.

I am also thankful to the members of the IceCube at Canterbury University especially postdoctoral fellow Mark Aartsen for his help and support throughout my research project. I thank to Sebastian Euler for supplying the majority of the initial code for the simulation of the extensive air shower.

Finally, I must express my gratitude to my family and friends for providing me support and encouragement through the process of researching and writing this thesis. This accomplishment would not have been possible without them.